8. Data Report: Paleomagnetic and Rock Magnetic Characterization of Rocks Recovered from Leg 173 Sites[1]

Xixi Zhao,[2] Brent D. Turrin,[3] Mike Jackson,[4] and Peter Solheid[4]

ABSTRACT

We present detailed paleomagnetic and rock magnetic results of rock samples recovered during Leg 173. The Leg 173 cores display a multi-component magnetization nature. Variations in magnetic properties correlate with changes in lithology that result from differences in the abundance and size of magnetic minerals. The combined investigation suggests that the magnetic properties of the "fresher" peridotite samples from Site 1070 are controlled mainly by titanomagnetite, with a strong Verwey transition in the vicinity of 110 K, and with field- and frequency-dependent susceptibility curves that resemble those of titanomagnetites. These results are in excellent agreement with thermomagnetic characteristics where titanomagnetites with Curie temperature ~580°C were identified from the "fresher" peridotites. In contrast to the magnetic properties observed from the "fresher" peridotites, the low-temperature curves for the "altered" peridotites did not show any Verwey transition. Thermomagnetic analysis using the high-temperature vibrating sample magnetometer also failed to show evidence for titanomagnetites. The remanent magnetization is carried by a thermally unstable mineral that breaks down at ~420°C, probably maghemite. The field- and frequency-dependent relationships are also directly opposite to those in the reversal zone, with no signs of titanomagnetite characteristics. Altogether, these rock magnetic data seem to be sensitive indicators of alteration and support the contention that maghemite is responsible for the magnetic signatures displayed in the altered peridotites of the upper section. The magnetic minerals of the basement rocks from Sites 1068, 1069, and 1070 are of variable particle

size but fall within the pseudo-single-domain size range (0.2–14 µm). The average natural remanent magnetization (NRM) intensity of recovered serpenitinized peridotite is typically on the order of 20 mA/m for samples from Site 1068, but ~120 mA/m for samples from Site 1070. The much stronger magnetization intensity of Site 1070 is apparently in excellent agreement with the observed magnetic anomaly high. Nearly half of the NRM intensity remained after 400°C demagnetization, suggesting that the remanence can contribute significantly to the marine magnetic anomaly.

INTRODUCTION

Ocean Drilling Program (ODP) Leg 173 was designed to further investigate the nature of basement within the ocean–continent transition zone (OCT) in the Iberia Abyssal Plain, off the west coast of Portugal. The main results of Leg 173 suggest that off west Iberia, basement in the OCT of the southern Iberia Abyssal Plain is made, at least sporadically, of peridotites over an east-west width of at least 95 km. The mantle rocks were unroofed in the continental breakup zone very close to the landward edge of the OCT, and the zone of mantle exposure in the OCT between the continental crust and the true oceanic crust is even more widespread than previously thought. However, no rocks of the upper oceanic crust (basaltic lavas or sheeted dikes) were found at Leg 173 sites. The nature and evolution of basement rocks as well as the horizontal extent of the serpentinized peridotite ridge within the OCT still remain unanswered or controversial.

Paleomagnetism continues to play a pivotal role as a standard for age dating and correlation in ODP studies. Paleomagnetic dating is based on the facts that the Earth's magnetic field occasionally reverses polarity and that many rocks retain a magnetic imprint of the field at the time they were formed or altered. Under favorable circumstances, paleomagnetic dating can furnish highly resolved numerical ages by identifying the polarity patterns and fitting the polarity patterns into biostratigraphically identified zones, the geomagnetic polarity time scale, or another geochronogical framework. Recently, measurement of rock magnetic parameters has been also demonstrated to be useful for studying various rock-forming and rock-altering geological processes. Rock magnetic properties can be used to identify the magnetic mineralogy and particle sizes, to subdivide or to correlate different sequences of the deposits, and to help assess the origin and stability of remanent magnetization. The combination of paleomagnetic and rock magnetic studies has importance in understanding the relationship of magnetic properties to the geological processes in the Iberia region and can help answer key questions such as what is the horizontal extent of the serpentinized peridotite ridge within the OCT.

The purpose of this paper is to present the results of such work conducted on cores recovered from Leg 173 sites. Below, we will first briefly introduce the background information about the study, followed by a description of the paleomagnetic and rock magnetic results from our own work to date with Leg 173 cores, focusing on the cores that provided the most readily interpretable data. We then discuss and summarize the data. Detailed data interpretations on peridotites and sediments, in conjunction with lithostratigraphy and other studies, have been submitted for publication to a special volume of Geologic Society

of London (Zhao, 2000) and as a synthesis paper for this volume (Zhao et al., **Chap. 11**, this volume).

BACKGROUND INFORMATION

Iberia separated from the Newfoundland margin of the Grand Banks during the Early Cretaceous after prolonged rifting that began during the Late Triassic (Wilson et al., 1989). The first quantitatively rigorous model that fits North America to Europe was performed by Bullard et al. (1965). They confirmed that, once the Bay of Biscay itself had been closed by a clockwise rotation of Iberia against Europe, the southeast Grand Banks margin could be matched with the west Iberia margin. Subsequently, more refined fits were obtained as seafloor spreading magnetic anomalies were identified between the two margins and in the Bay of Biscay (Le Pichon et al., 1977; Courtillot, 1982; Masson and Miles, 1984; Klitgord and Schouten, 1986; Srivastava and Tapscott, 1986; Srivastava and Verhoef, 1992; Sibuet and Srivastava, 1994). The west Iberia margin is a nonvolcanic rifted margin characterized by an apparent lack of synrift volcanism. Scientific drilling of the OCT off the west Iberia margin was first conducted during Leg 103 in 1985 (Boillot, Winterer, Meyer, et al., 1987). During this leg, a short transect of holes was drilled west of Galicia Bank (Sites 637–641; Fig. **F1**). In 1993 during Leg 149, a west-to-east transect of five sites in the OCT was drilled west of the Iberia margin (Sites 897–901, see inset in Fig. **F1**). At three of these sites (Sites 897, 899, and 900), acoustic basement was reached and a sequence of serpentinized peridotite and associated mantle rocks were recovered from the basement (Sawyer, Whitmarsh, Klaus, et al., 1994; Alt and Shanks, 1998). A fourth site (Site 901) enabled a firm prediction that the underlying basement is continental crust. Leg 173 is a sequel to Leg 149. A total of five sites were drilled during Leg 173 in 1997 (Sites 1065, 1067, 1068, 1069, and 1070; see Fig. **F1**). Basement rocks at three of the five sites (Sites 1067, 1068, and 1070) featured a complex exposure of mantle rocks including serpentinized peridotite, alternating tectonic breccia, and amphibolite-grade metagabbro (Whitmarsh, Beslier, Wallace, et al., 1998). Petrologic changes in these basement rocks most likely correlate with the processes of breakup of Iberia from Newfoundland and the onset of steady-state seafloor spreading. The enigmatic J anomaly (bold line in Fig. **F1**), which has been shown in the central Atlantic to be 120–125 m.y. old (Tucholke and Ludwig, 1982), is identified from just west of Site 1070 (only 15 km). The results from Legs 149 and 173 both have proved the existence of a north-south-trending serpentinized peridotite ridge in the OCT of the southern Iberia Abyssal Plain. This ridge may extend, with en echelon offsets, along the margin for ~300 km. No evidence exists to suggest that faulting activity in the region produced the offset ridges. Such a distribution of the peridotite makes the peridotite ridges in the western Iberia margin one of the most enigmatic elements in the geologic history of the region (Whitmarsh et al., 1996; Whitmarsh, Beslier, Wallace, et al., 1998). In addition, these ridges are parallel to the seafloor-spreading isochrons to the west and possess remanent magnetization with a Cretaceous declination (Discovery 215 Working Group, 1998), indicating that they were formed by seafloor spreading. It appears that the OCT, however formed, is much narrower off Galicia Bank at the north end of the peridotite ridge. The full consequence of the peridotite ridge formation is only just beginning to be appreciated and is far from being understood. The

F1. Regional bathymetric chart and cross section of the west Iberia margin, p. 15.
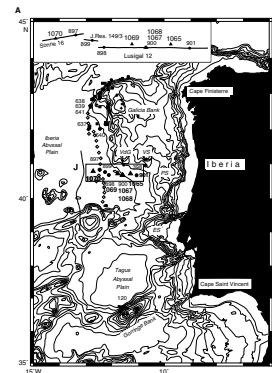
intimate coexistence between the marine magnetic anomaly and the margin-parallel peridotite ridge implies an integrated dynamic process and may contain clues to our understanding of the rifting process.

SITE SETTING

The site locations (Fig. F1) and the structure and morphology of the drilling sites are documented in detail in site chapters of the Initial Reports of the Proceedings of the Ocean Drilling Program Volume 173 and other appropriate papers (see Whitmarsh, Beslier, Wallace, et al., 1998) and will be only briefly summarized here. Site 1065, in a tilted fault block, was chosen to be drilled deep enough to reach igneous or metamorphic rocks to determine whether the block consisted of continental crust. Site 1067, which lies near the northern edge of the southern Iberia Abyssal Plain was chosen to investigate the nature of the H reflector. After technical problems prevented us from reaching the reflector and underlying terrane at Site 1067, Site 1068 was chosen at the southern edge of the Iberia Abyssal Plain with the primary objective of sampling the crystalline basement just to the west of Sites 1067 and 900. Site 1069 is situated in the southern Iberia Abyssal Plain in a location where a variety of structural and geophysical models for the development of the OCT can be tested. Finally, Site 1070 lies ~15 km east of the crest of the J magnetic anomaly and 20 km west of the peridotite ridge, as mentioned above. The main objective at this site was to sample basement at the western end of the OCT where oceanic crust is inferred by geophysical data. The peridotite recovered at this site has suffered low-temperature and late-stage alteration. One most obvious visible feature resulting from this alteration is the color variation. At Site 1070, the upper part of the peridotite section is pervasively oxidized serpentinites and altered to a brown-colored or yellowish green serpentinized peridotite and breccia. The lower part of the peridotite section consists of "fresher" (compared to that of the upper part of the section) serpentinized peridotites, generally dark gray or greenish black. For the purpose of convenience, the terms "altered" and "fresher" peridotites are used in various sections of this paper.

LABORATORY AND ANALYTICAL METHODS

Paleomagnetic Sampling

During Leg 173, a total of 602 discrete paleomagnetic samples were taken for shipboard and shore-based paleomagnetic and rock magnetic studies. These 2.5-cm cylindrical samples were drilled from the core sections that contained vertically oriented long pieces, using a water-cooled nonmagnetic drill bit attached to a standard drill press. In all cases, the uphole direction was carefully recorded on the sample by means of an orientation arrow before removal from the core section. All samples were kept in a low-field environment (field-free room) to prevent viscous remanence acquisition.

Magnetic Measurement Procedure

The paleomagnetic and rock magnetic data presented in this paper are of two different types: those obtained using the shipboard pass-

through cryogenic magnetometer and those derived from analysis of discrete samples both on ship and on shore. In the shipboard pass-through system, magnetic measurements were performed by passing continuous archive-half core sections through a 2G cryogenic magnetometer. Measurements were taken at intervals of either 5 or 10 cm along the core, after alternating field (AF) demagnetization at 10 and 15 mT. Whole-core magnetic susceptibility was measured at 3-cm intervals on selected sections using the Bartington ms2 susceptibility meter mounted on the multisensor track. A total of 188 samples were stepwise demagnetized during the cruise using Schonstedt equipment to evaluate the directional stability and coercivity/unblocking temperature spectra of each sample, and 415 samples were set aside to the first author for further rock magnetic and demagnetization analysis at the University of California at Santa Cruz (UCSC). During thermal demagnetization, the initial susceptibility was monitored between each temperature step as a means of assessing any irreversible mineralogical changes associated with heating. A vector diagram was used for each sample to identify the magnetic components of magnetization that were present. Magnetic components were determined by fitting least-squares lines to segments of the vector demagnetization plots or "the principal component analysis" (Zijderveld, 1967; Kirschvink, 1980) that were linear in three-dimensional space.

Rock magnetic measurements of discrete samples in shore-based studies were performed at the paleomagnetism laboratories at UCSC and at the Institute for Rock Magnetism of the University of Minnesota. For rock magnetic characterization, samples were subjected to a wide range of magnetic measurements. These included (1) the initial natural remanent magnetization (NRM) measurement followed by 2 weeks of zero-field storage; (2) remeasurement of NRM; (3) initial susceptibility; (4) Koenigsberger ratio; (5) hysteresis loop parameters: saturation magnetization (J_s), saturation remanence (J_r), coercivity (H_c), remanent coercivity (H_{cr}); (6) thermomagnetic measurements, that is, low-temperature (5 and 10 K) thermal demagnetization of saturation isothermal remanent magnetization and high-temperature (up to 700°C) dependence of the magnetic moment and Curie temperature determination; and (7) alternating current (AC) susceptibility measurements as a function of field amplitude and of frequency. Results of each experiment are given in the section below.

MAGNETIC RESULTS

The results of measurements 1 through 5 (see preceding paragraph) are given in Tables T1 and T2. Measurements 6 and 7 are discussed separately.

Remanence Properties

Whole-Core Pass-Through Measurement: Natural Remanent Magnetization Intensity and Magnetic Susceptibility

Within the five drilling sites (1065, 1067, 1068, 1069, and 1070), where rock magnetic screening of samples was made, there are considerable variations in magnetic properties and demagnetization behavior among the various lithologies, which will be described elsewhere. The most common features, however, can be summarized as follows: A re-

magnetization imparted by the coring process is commonly encountered as noted during previous legs (e.g., Gee et al., 1989; Zhao et al., 1994). This remagnetization is characterized by NRM inclinations that are strongly biased toward vertical value (+90°) in many cores. This remagnetization most severely affected the external portions of the cores (presumably because the outside of the core is physically closer to the magnetized core barrel). As shown in Figures **F2** and **F3,** upon demagnetization to 60 mT, a significant decrease in intensity and a shift of inclination toward negative values were observed, suggesting the presence of drilling-induced remagnetization. At all Leg 173 sites, variations in magnetic susceptibility generally parallel the variations in NRM intensity (e.g., see Fig. **F2**). The general trend of the susceptibility data curve was used to characterize the magnetic material contained within the cored material and for correlating sedimentary intervals between selected drilled sites. A good example was presented during shipboard study (Shipboard Scientific Party, 1998, p. 207) where sections of magnetic susceptibility profiles from Holes 1068A and 1067A can be correlated.

AF and Thermal Demagnetization of Discrete Samples

To investigate the nature of the remanent magnetization of the discrete samples from Leg 173 sites, selected samples were stepwise AF or thermally demagnetized. The NRM intensity or direction of the minicore samples did not change significantly (<5%) after zero-field storage for 2 weeks. As mentioned above, the vertically directed drilling-induced magnetization is often present in Leg 173 cores. In most cases, this steeply downward component of magnetization is not very resistant to AF demagnetization (e.g., see Fig. **F4A**). Thermal demagnetization of minicore samples also successfully removed this drilling-induced magnetization component (Fig. **F4B**). As shown in Figure **F4B,** the drilling-induced remagnetization component (with inclination >75°) is removed after 250°C demagnetization and a characteristic component (with inclination ~50°) can be identified. As mentioned, we used magnetic susceptibility to monitor the production of new magnetic materials during thermal demagnetization that might have altered the remanence. Apart from small, insignificant fluctuations, the susceptibility of minicore samples generally did not change until after they had been heated to 350°C. Above this temperature, many samples showed a decrease or increase in susceptibility. In addition, progressive thermal demagnetization on several minicores of metasediments and serpentinized peridotite revealed that a component of viscous remagnetization (VRM) parallel to the present-day magnetic field has been recorded in these rocks. The measured VRM has been demonstrated to be useful for orienting cores for structural studies (see the Site 1067–1070 chapters in Whitmarsh, Beslier, Wallace, et al., 1998). Examples of this VRM application are given in Table **T3.**

Results from AF and thermal demagnetization of basement samples from Sites 1067, 1068, and 1070 show behavior that cannot be interpreted in such a simple fashion. As shown in Figure **F5,** some of these basement samples exhibited signs of drilling-induced magnetization as evidenced by the steep inclinations in the initial demagnetization measurements (AF demagnetization to 15 mT effectively removed this overprint; see Fig. **F5A**). Others show a "soft" VRM component that was removed at low-temperature demagnetization steps (NRM = 300°C), followed by a stable component of magnetization (300° to 566°C de-

F2. Plot of remanent intensity before and after AF demagnetization and volume magnetic susceptibility all as a function of depth, p. 17.
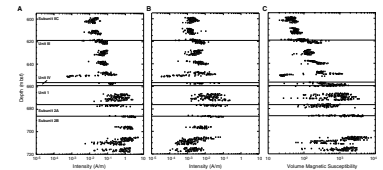
F3. Downhole variation of magnetic inclination before and after AF demagnetization, p. 18.
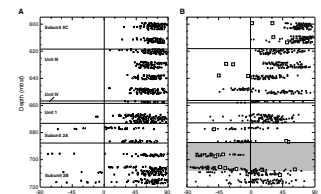
F4. Representative vector endpoint diagrams of results of AF demagnetization and thermal demagnetization, p. 19.
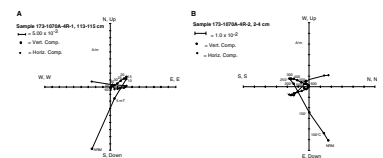
T3. Structural and magnetic data from the basement Subunit 1B, p. 34.

F5. Representative vector endpoint diagrams of results of AF demagnetization and thermal demagnetization, p. 21.
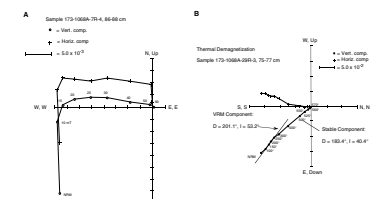
magnetization; see Fig. F5B). Although not every section was sampled and measured, it seems reasonable to conclude that drilling has had a lesser effect on the NRM of basement samples as compared with that of sedimentary cores.

It is interesting to note that the stable component for serpentinized peridotite samples from Site 1068 has a much shallower inclination compared to the expected inclination at the drilling site. The magnetically cleaned inclinations (mean = 42.9°; N = 17; α_{95} = 3.7°) in the serpentinized peridotites are systematically shallower than the inclination expected today (59°) at the drilling sites but are statistically indistinguishable from the Jurassic–Cretaceous inclinations for Iberia (33.4°–45.2° and α_{95} ~10°; see Van der Voo, 1969; Galdeano et al., 1989). A similar observation was also made in serpentinized peridotites from Site 1070. Assuming the inclination represents the primary remanence at the time when these rocks were formed, the similarity between the observed and the expected inclinations is consistent with the notion that the drill sites were part of the Iberia plate at the time of acquisition of the magnetization. Alternatively, the shallow inclination could indicate that these sections have been tilted after the acquisition of the magnetization, or a combination of both.

Koenigsberger Ratio

The Koenigsberger ratio, Q, is defined as the ratio in a rock of remanent magnetization to the induced magnetization in the Earth's field. In general, the Koenigsberger ratio is used as a measure of the stability to indicate a rock's capability of maintaining a stable remanence. The International Geomagnetic Reference Field value at the Leg 173 site (45,000 nT = 35.83A/m) was used for calculating Q, where

$$Q = \text{NRM (A/m)}/(k \, [\text{SI}] \times H \, [\text{A/m}])$$

and H is the local geomagnetic field. The variation of the Koenigsberger ratios in Table T1 in general resembles that of the NRM. For example, the serpentinized peridotite samples from Site 1070 have a higher intensity of remanence than the overlying sedimentary rocks, and consequently the Koenigsberger ratio of the former is higher than that of the latter. Similar examples of this correlation are also seen in samples from other Leg 173 sites. The Koenigsberger ratios for many claystone and nannofossil chalk samples from Leg 173 sites are <1.0, indicating that induced magnetization would be more than or comparable to remanent magnetization. The low value of the Koenigsberger ratio for these samples also indicates the presence of low-coercivity magnetic minerals that carry an unstable remanence and are more susceptible to an external magnetic field. The other parameters measured are the median-demagnetizing field or the unblocking temperature (T_b), both of which represent the stability of remanence.

Low-Field Magnetic Susceptibility

Volume magnetic susceptibility of natural materials in a weak magnetic field depends on the abundance and grain size of ferromagnetic minerals. As listed in Table T1, discrete samples of sedimentary rocks show low magnetic susceptibility values, indicating a very low concentration of ferro(i)magnetic minerals in these rocks. The susceptibility of serpentinized peridotite samples from Sites 1067, 1068, and 1070, on

the other hand, is much higher than that of the overlying sediments. This is expected because they are known to have very different magnetic mineralogies. In this study, initial susceptibility was often routinely measured after each measurement step during thermal demagnetization in order to monitor changes in magnetic mineralogy during heating. For example, maghemite to hematite transition at ~300°C produces a decrease in susceptibility, which is a useful means of identifying the presence of this mineral (Opdyke and Channell, 1996).

Rock Magnetic Properties

Hysteresis Loop Parameters

Saturation magnetization (J_s), saturation remanence (J_r), coercive force (H_c), and remanent coercivity (H_{cr}, from back-field experiments) are parameters that can be determined from a hysteresis loop. Hysteresis loop parameters are useful in characterizing the intrinsic magnetic behavior of rocks. Thus, they are helpful in studying the origin of remanence. In this study, hysteresis loops and the associated parameters J_r/J_s, H_c, and H_{cr} were obtained using an alternating gradient magnetometer (Princeton Measurements Corporation) capable of resolving magnetic moments as small as 5×10^{-8} emu (Flanders, 1988). Hysteresis parameters determined from 12 representative samples from Leg 173 sites are presented in Table T2. Saturation magnetization (J_s) is a measure of the total amount of magnetic mineral in the sample. The coercivity, H_c, is a measure of magnetic stability. The two ratios, J_r/J_s and H_{cr}/H_c, are commonly used as indicators of domain states and, indirectly, grain size. For magnetite, high values of J_r/J_s (>0.5) indicate small (<0.1 µm or so) single-domain (SD) grains, and low values (<0.1) are characteristic of large (>15–20 µm) multidomain (MD) grains. The intermediate regions are usually referred to as pseudo–single domain (PSD). H_{cr}/H_c is a much less reliable parameter, but conventionally SD grains have a value close to 1.1, and MD grains should have values >3–4 (Day et al., 1977). Figure F6 displays the ratios of the hysteresis parameters for Leg 173 samples containing mainly titanomagnetite as magnetic minerals plotted on a Day et al. (1977)-type diagram. Such a representation provides qualitative information on the magnetic grain sizes from SD to PSD to large MD. The samples analyzed in this study indicate that the magnetic grain sizes of the Site 1069 samples fall near the boundary between SD and PSD, whereas the samples from Sites 1070 and 1068 are in the PSD range. The Fe-Ni metal Sample 173-1068A-26R-4W, 18–20 cm (awaruite), is an exception that falls in the MD region. Hysteresis behavior of three yellow chalk samples from Site 1069 and two amphibolite breccia samples from Site 1067 were also studied, but the results are complex and are not readily explained at present.

Low-Temperature Properties

Transitions in the magnetic properties of magnetite, pyrrhotite, and hematite occur at low temperatures and they provide a potential means of magnetic mineral identification. Magnetite exhibits a crystallographic phase transition from cubic to monoclinic at 110–120 K. Associated with this transition, the anisotropy constant goes through zero as the easy axis of magnetization changes from [100] to [111] (Nagata et al., 1964). Low-temperature measurements were made on 16 represen-

F6. Hysteresis ratios plotted on a diagram, p. 22.
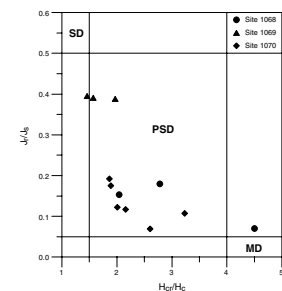
tative samples to help characterize the magnetic minerals and understand their rock magnetic properties. These measurements were designed to determine the Néel temperature and other critical temperatures of a magnetic substance and were made from 10 K to room temperature on 100–300 mg subsamples in a Quantum Design Magnetic Property Measurement System (MPMS) at the University of Minnesota. By definition, a ferrimagnetic mineral grain is superparamagnetic if its volume is smaller than the critical value 25 kT/K (where k = Boltzmann's constant, T = 300 K in this study, and K = the magnetic anisotropy constant per unit volume), so that its net remanence over 100 s is zero (Cullity, 1972). However, as T is decreased toward 0 K, the thermal energy kT decreases and K increases (both serving to aid magnetic stability) so that all grains that were superparamagnetic at 300 K will be able to retain thermally stable remanent magnetization near 0 K (Banerjee et al., 1992). The so-called Verwey transition in magnetite can be observed by a decrease in intensity of an IRM at low temperature as it is allowed to warm through or cool through the transition temperature. In this study, these experiments included (1) cooling the sample from room temperature (300 K) down to 10 K (in some cases to 5 K) in a steady magnetic field of 2.5 T and measuring the remanence at 5 K intervals; (2) measuring the saturation isothermal remanence magnetization (SIRM) at 5 and 10 K (SIRM5 and SIRM10, respectively) and then warming it to 300 K in zero field while measuring the remanence value every 5 K.

As shown in Figure F7, the low-temperature curves of SIRM both in zero-field warming and in a 2.5 T field cooling display a variety of features. These include an unblocking temperature in the vicinity of 40–60 K, most likely caused by ferrimagnetic pyrrhotite or greigite (Dekkers et al., 1989; Rochette et al., 1990) and a decrease in remanence in the 100–120 K range, most likely caused by the magnetocrystalline anisotropy constant, k$_1$, of magnetite going to zero in this temperature, known as the Verwey transition (Verwey et al., 1947). The low-temperature data are one of the major lines of evidence for the presence of Fe-Ni metals in Site 1068 peridotite, (titano)magnetites in the "fresher" peridotites of Site 1070, and maghemites in the "altered" part of the peridotite section (Zhao, 2000).

Curie Temperature

Curie temperature is the temperature below which a magnetic mineral is magnetically ordered. Because this value is a sensitive indicator of composition, it is useful in understanding the magnetic mineralogy. In this study, Curie temperature was determined by measurement of magnetic moment vs. temperature (using the Princeton MicroMag Vibrating Sample Magnetometer at the University of Minnesota), because the magnetic moment drops to zero about the Curie temperature. We conducted thermomagnetic analyses in an inert atmosphere on 16 samples chosen to be representative of the Leg 173 cores.

Figure F8 shows high-temperature magnetic moment runs of a representative "altered" and a "fresher" peridotite sample from Site 1070. The heating and cooling curves for the "altered" sample display a significant drop of magnetic moment ~420°C (Fig. F8A). This drop may be indicative of a fraction of maghemite, which could be responsible for the observed remanent magnetization. For the "fresher" peridotite sample, the results show Curie temperatures between 550° and 580°C, indicative of the presence of titanomagnetite (Fig. F8B).

F7. Low-temperature heating curves of saturation remanence normalized for several representative samples, p. 23.
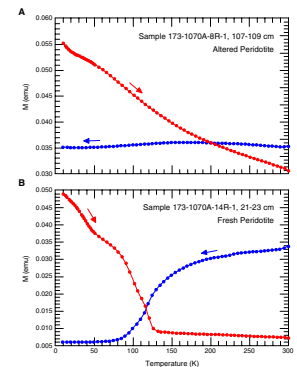
F8. Typical thermomagnetic curves for Leg 173 peridotites, p. 25.
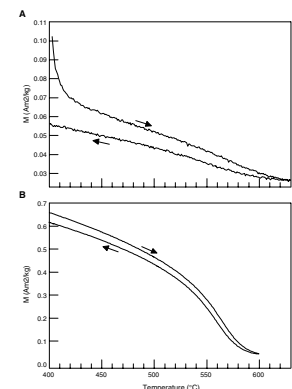
Low-Temperature AC Susceptibility Measurements

In a nonlinear and sinusoidally varying applied field, the magnetic response is determined by factors including field dependence and time or frequency dependence (i.e., viscosity) (Jackson et al., 1998). Previous work by Worm et al. (1993) and Jackson et al. (1998) has suggested that ferrimagnetic pyrrhotite and titanomagnetites exhibit strong field dependence of AC susceptibility in a large applied field. To investigate the field- and frequency-dependent susceptibility of the Leg 173 cores, AC susceptibility measurements were made on selected samples with a LakeShore Model 7130 AC susceptometer at the University of Minnesota. The temperature dependence of the in-phase (κ') susceptibility between 15–300 K was measured at two frequencies (95 and 1000 Hz), with AC field amplitudes between 100 and 1000 A/m.

The main observations in this study can be outlined as follows:

1. The field- and frequency-dependent susceptibility curves for the "fresher" peridotites from Site 1070 are similar to those of synthetic titanomagnetite 55 (TM55) (Jackson et al., 1998), with some field dependence and no frequency dependence.
2. For the "altered" peridotite, the field- and frequency-dependent relationships are directly opposite to those in the "fresher" zone, with some frequency dependence but no field dependence.
3. There is no detectable frequency dependence of susceptibility or its field dependence for these awaruite-bearing samples from Site 1068, probably because their susceptibility is a superposition of paramagnetic, antiferromagnetic, and ferrimagnetic susceptibilities from different Fe-bearing phases.

Figure F9 shows an example of the temperature dependence of magnetic susceptibility between 15 and 300 K for an "altered" peridotite sample. More examples and detailed descriptions can be found in Zhao (2000).

DISCUSSION

The Leg 173 cores recovered from the five drilling sites displayed a multicomponent nature of magnetization. The steep, positive drilling-induced component is evident in almost all samples. Variations of the Koenigsberger ratio and the initial magnetic susceptibilities generally resemble those of NRMs. Both the NRM intensity and the magnetic susceptibility are parameters that likely reflect variations in type and amount of magnetic minerals within the drilling sites. The averaged NRM intensity of recovered serpentinized peridotite is typically on the order of 20 mA/m for samples from Site 1068 but ~120 mA/m for samples from Site 1070. A recent magnetic survey revealed that there is a magnetic anomaly high (~0.3 A/m) in the vicinity of Site 899, which was ~40 km eastward and was previously thought to result from a relatively strongly magnetized nonoceanic crust (Whitmarsh et al., 1996; Discovery 215 Working Group, 1998). The much stronger magnetization intensity of Sites 899 and 1070 are apparently in excellent agreement with the observed magnetic anomaly high, suggesting that the serpentinized peridotite body under Site 899 and Site 1070 contribute significantly to the magnetic anomaly. In several samples in Hole 1070A nearly half of the NRM intensity remained after 400°C demagne-

F9. Representative diagram showing the temperature dependence of mass susceptibility for an altered peridotite sample, p. 26.
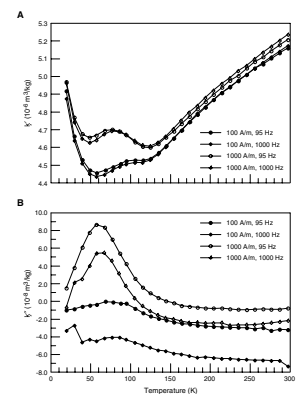
tization, suggesting the remanence can contribute significantly to the anomaly.

Stable components of magnetization are revealed in the results of demagnetization on Leg 173 samples (Table T1). A number of magnetic polarity reversals may be discerned on the basis of changes in sign of the characteristic inclinations from samples in Sites 1068, 1069, and 1070. These samples maintain inclinations close to the theoretically predicted values for the paleolatitude of drilling sites, indicating they may represent the primary magnetization. A magnetostratigraphy from middle Eocene to late Cretaceous for sediments cored at Site 1068 was established and presented in a synthesis paper (Zhao et al., Chap. 11, this volume).

Results from low-temperature measurements in the MPMS (high-field = 2.5T) and LakeShore (low-fields = 100–1000 A/m) susceptometers show that (titano)magnetites are present in the "fresher" peridotites, with a strong Verwey transition in the vicinity of 110 K, and with field- and frequency-dependent susceptibility curves that resemble those of synthetic TM55. These results are in good agreement with the thermomagnetic characteristics where titanomagnetites with Curie temperatures around 580°C were identified from the "fresher" peridotites. The hysteresis ratios suggest that the bulk magnetic grain size is in the PSD boundary (e.g., with lower H_{cr}/H_c values). In contrast to the magnetic properties observed from the "fresher" peridotites, the low-temperature curves for the "altered" peridotites did not show any Verwey transition. Thermomagnetic analysis using the high-temperature vibrating sample magnetometer also failed to show evidence for titanomagnetites. The remanent magnetization is carried by a thermally unstable mineral that breaks down at ~420°C, probably maghemite. The field- and frequency-dependent relationships are also directly opposite to those in the reversal zone, with no signs of titanomagnetite characteristics. Although the hysteresis ratios still fall in the PSD region, the cluster is centered toward the multidomain region (with higher H_{cr}/H_c ratios). Altogether, these rock magnetic data seem to be sensitive indicators of alteration and support the contention that maghemite is responsible for the magnetic signatures displayed in the altered peridotites of the upper part of the peridotite section. The rock magnetic properties are useful in evaluating the fidelity of the natural magnetic memory in upper mantle rocks and in understanding the alteration processes through time.

To sum up, the results described above have revealed important information about the origin of remanence and on the magnetic minerals present in the Leg 173 cores, which in turn provide physical insight into the geodynamic evolution of the Iberia margin (from continental rifting to seafloor spreading). Much more additional work is needed to prove or disprove various possibilities and constrain the magnetic interpretation.

CONCLUSIONS

Preliminary paleomagnetic study has revealed important magnetic signatures that await further verification in terms of age and origin. Although more basic rock magnetic and isotopic data are still needed to be able to interpret the remarkable magnetic behavior of the Iberia peridotites, significant progress was already made during our postcruise study to narrow down the possible explanations. The following are the

conclusions drawn from our comprehensive examination of the remanence magnetization and magnetic mineralogy of Leg 173 cores:

1. The combined investigation suggests that the magnetic properties of the fresher and altered peridotite samples from Site 1070 are controlled mainly by titanomagnetite and maghemite, respectively. This study verifies that the low-temperature magnetic phase transitions are effective means of detecting the presence of minor magnetic minerals.
2. The magnetic minerals of the basement rocks from Sites 1068, 1069, and 1070 are of variable particle size but fall within the pseudo–single domain size range (0.2–14 µm).
3. The averaged NRM intensity of recovered serpentinized peridotite is on the order of 120 mA/m for samples from Site 1070. Significant amount of NRM intensity remains after 400°C thermal demagnetization, suggesting the remanence can contribute significantly to the observed marine magnetic anomaly high.
4. It is clear from this study that a combination of paleomagnetic and rock magnetic studies on the same cores can provide important information that has considerable relevance to understanding the evolution of the Iberia margin. This study has demonstrated the potential value of paleomagnetic, rock magnetic, and geological investigations in providing the essential link between magnetic property variations and the extent of mineral alteration.

ACKNOWLEDGMENTS

REFERENCES

Alt, J.C., and Shanks, W.C., 1998. Sulfur in serpentinized oceanic peridotite: serpentinization processes and microbial sulfate reduction. *J. Geophys. Res.,* 103:9917–9929.

Banerjee, S.K., 1992. Applied rock magnetism in the 1990's: potential breakthrough in a new user-driven science. *Eos,* 73:142–143.

Beslier, M.O., Ask, M., and Boillot, G., 1993. Ocean-continent boundary in the Iberia abyssal plain from multichannel seismic data. *Tectonophysics,* 218:383–393.

Boillot, G., Winterer, E.L., et al., 1988. *Proc. ODP, Sci. Results,* 103: College Station, TX (Ocean Drilling Program).

Bullard, E., Everett, J.E., and Smith, A.G., 1965. The fit of the continents around the Atlantic. *Philos. Trans.R. Soc. London A,* 258:41–75.

Courtillot, V., 1982. Propagating rifts and continental breakup. *Tectonics,* 1:239–250.

Cullity, B.D., 1972. *Introduction to Magnetic Materials:* Reading, MA (Addison-Wesley).

Day, R., Fuller, M., and Schmidt, V.A., 1977. Hysteresis properties of titanomagnetites: grain-size and compositional dependence. *Phys. Earth Planet. Inter.,* 13:260–267.

Dekkers, M.J., Mattei, J.-L., Fillion, G., and Rochette, P., 1989. Grain-size dependence of the magnetic behavior of pyrrhotite during its low-temperature transition at 34K. *Geophys. Res. Lett.,* 16:855–858.

Discovery 215 Working Group, 1998. Deep structure in the vicinity of the ocean-continent transition zone under the southern Iberia Abyssal Plain. *Geology,* 8:743–746.

Flanders, P.J., 1988. An alternating-gradient magnetometer. *J. Appl. Phys.,* 63:3940–3945.

Galdeano, A., Moreau, M.G., Pozzi, J.P., Berthou, P.Y., and Malod, J.A., 1989. New paleomagnetic results from Cretaceous sediments near Lisboa (Portugal) and implications for the rotation of Iberia. *Earth Planet. Sci. Lett.,* 92:95–106.

Gee, J., Staudigel, H., and Tauxe, L., 1989. Contribution of induced magnetization to magnetization of seamounts. *Nature,* 342:170–173.

Jackson, M.J., Moskowitz, B.M., Rosenbaum, J., and Kissel, C., 1998. Field-dependence of AC susceptibility in titanomagnetites. *Earth Planet. Sci. Lett.,* 157:129–139.

Kirschvink, J.L., 1980. The least-squares line and plane and the analysis of palaeomagnetic data. *Geophys. J. R. Astron. Soc.,* 62:699–718.

Klitgord, K.D., and Schouten, H., 1986. Plate kinematics of the central Atlantic. *In* Vogt, P.R., and Tucholke, B.E. (Eds.), *The Geology of North America* (Vol. M): *The Western North Atlantic Region.* Geol. Soc. Am., 351–378.

Le Pichon, X., Sibuet, J.C., and Francheteau, J., 1977. The fit of the continents around the North Atlantic Ocean. *Tectonophysics,* 38:169–209.

Masson, D.G., and Miles, P.R., 1984. Mesozoic seafloor spreading between Iberia, Europe and North America. *Mar. Geol.,* 56:279–287.

Nagata, T., Kobayashi, K., and Fuller, M., 1964. Identification of magnetite and hematite in rocks by magnetic observation at low temperature. *J. Geophys. Res.,* 69, 2111–2120.

Opdyke and Channell, 1996. *Magnetic stratigraphy,* International Geophysics Ser., 64 (Academic Press).

Rochette, P., Fillion, G., Mattéi, J.-L., and Dekkers, M.J., 1990. Magnetic transition at 30–34 Kelvin in pyrrhotite: insight into a widespread occurrence of this mineral in rocks. *Earth Planet. Sci. Lett.,* 98:319–328.

Sawyer, D.S., Whitmarsh, R.B., Klaus, A., et al., 1994. *Proc. ODP, Init. Repts.,* 149: College Station, TX (Ocean Drilling Program).

Shipboard Scientific Party, 1998. Site 1068. *In* Whitmarsh, R.B., Beslier, M.-O., Wallace, P.J., et al., *Proc. ODP, Init. Repts.,* 173: College Station, TX (Ocean Drilling Program), 163–218.

Sibuet, J.-C., and Srivastava, S., 1994. Rifting consequences of three plate separation. *Geophys. Res. Lett.,* 21:521–524.

Srivastava, S.P., and Tapscott, C.R., 1986. Plate kinematics of the North Atlantic. *In* Vogt, P.R., and Tucholke, B.E. (Eds.), *The Western North Atlantic Region.* Geol. Soc. Am., Geol. North Am. Ser., M:379–404.

Srivastava, S.P., and Verhoef, J., 1992. Evolution of Mesozoic sedimentary basins around the North Central Atlantic: a preliminary plate kinematic solution. *In* Parnell, J. (Ed.), *Basins of the Atlantic Seaboard: Petroleum Geology, Sedimentology and Basin Evolution.* Geol. Soc. Spec. Publ. London, 62:397–420.

Tucholke, B.E., and Ludwig, W.J., 1982. Structure and origin of the J anomaly Ridge, western North Atlantic Ocean. *J. Geophys. Res.,* 87:9389–9407.

Van der Voo, R., 1969. Paleomagnetic evidence for the rotation of the Iberia peninsula. *Tectonophysics,* 7:5–56.

Verwey, E.J., Haayman, P.W., and Romeijn, F.C., 1947. Physical properties and cation arrangements of oxides with spinal structure. *J. Chem. Phys.,* 15:181–187.

Whitmarsh, R.B., Beslier, M.-O., Wallace, P.J., et al., 1998. *Proc. ODP, Init. Repts.,* 173: College Station, TX (Ocean Drilling Program).

Whitmarsh, R.B., Miles, P.R., Sibuet, J.-C., and Louvel, V., 1996. Geological and geophysical implications of deep-tow magnetometer observations near Sites 897, 898, 899, 900, and 901 on the west Iberia continental margin. *In* Whitmarsh, R.B., Sawyer, D.S., Klaus, A., and Masson, D.G. (Eds.), *Proc. ODP, Sci. Results,* 149: College Station, TX (Ocean Drilling Program), 665–674.

Wilson, R.C.L., Hiscott, R.N., Willis, M.G., and Gradstein, F.M., 1989. The Lusitanian Basin of west-central Portugal: Mesozoic and Tertiary tectonic, stratigraphic and subsidence history. *In* Tankard, A.J., and Balkwill, H.R. (Eds.), *Extensional Tectonics and Stratigraphy of the North Atlantic Margins.* AAPG Mem., 46:341–361.

Worm, H.-U., Clark, D., and Dekkers, M.J., 1993. Magnetic susceptibility of pyrrhotite: grain size, field and frequency dependence. *Geophys. J. Int.,* 114:127–137.

Zhao, X., in press. Paleomagnetic and rock magnetic results from serpentinized peridotites beneath the Iberia Abyssal Plain. *In* Wilson, R.C.L., Beslier M.-O., Whitmarsh, R.B., Froitzheim, N., and Taylor, B. (Eds.), *Non-volcanic Rifting of Continental Margins: A Comparison of Evidence From Land and Sea.* Geol. Soc. Spec. Publ. London.

Zhao, X., Roperch, P., and Stokking, L.B., 1994. Magnetostratigraphy of the North Aoba Basin. *In* Greene, H.G., Collot, J.-Y., Stokking, L.B., et al., *Proc. ODP, Sci. Results,* 134: College Station, TX (Ocean Drilling Program), 457–474.

Zijderveld, J.D.A., 1967. AC demagnetization of rocks: analysis of results. *In* Collinson, D.W., Creer, K.M., and Runcorn, S.K. (Eds.), *Methods in Palaeomagnetism:* New York (Elsevier), 254–286.

Figure F1. A. Regional bathymetric chart of the west Iberia margin showing the ODP drilling transect along latitude 40°40′N (rectangle). Triangles = Leg 173 sites, dots = Leg 149 sites, numbered dots = earlier DSDP/ODP sites. The inset shows the locations of all sites on the transect. The line labeled J = the crest of the J magnetic anomaly. Open diamonds = the locus of the peridotite ridge (after Beslier et al., 1993). VDG = Vasco da Gama Seamount, VS = Vigo Seamount, PS = Porto Seamount, ES = Estremadura Spur. (Continued on next page.)

A
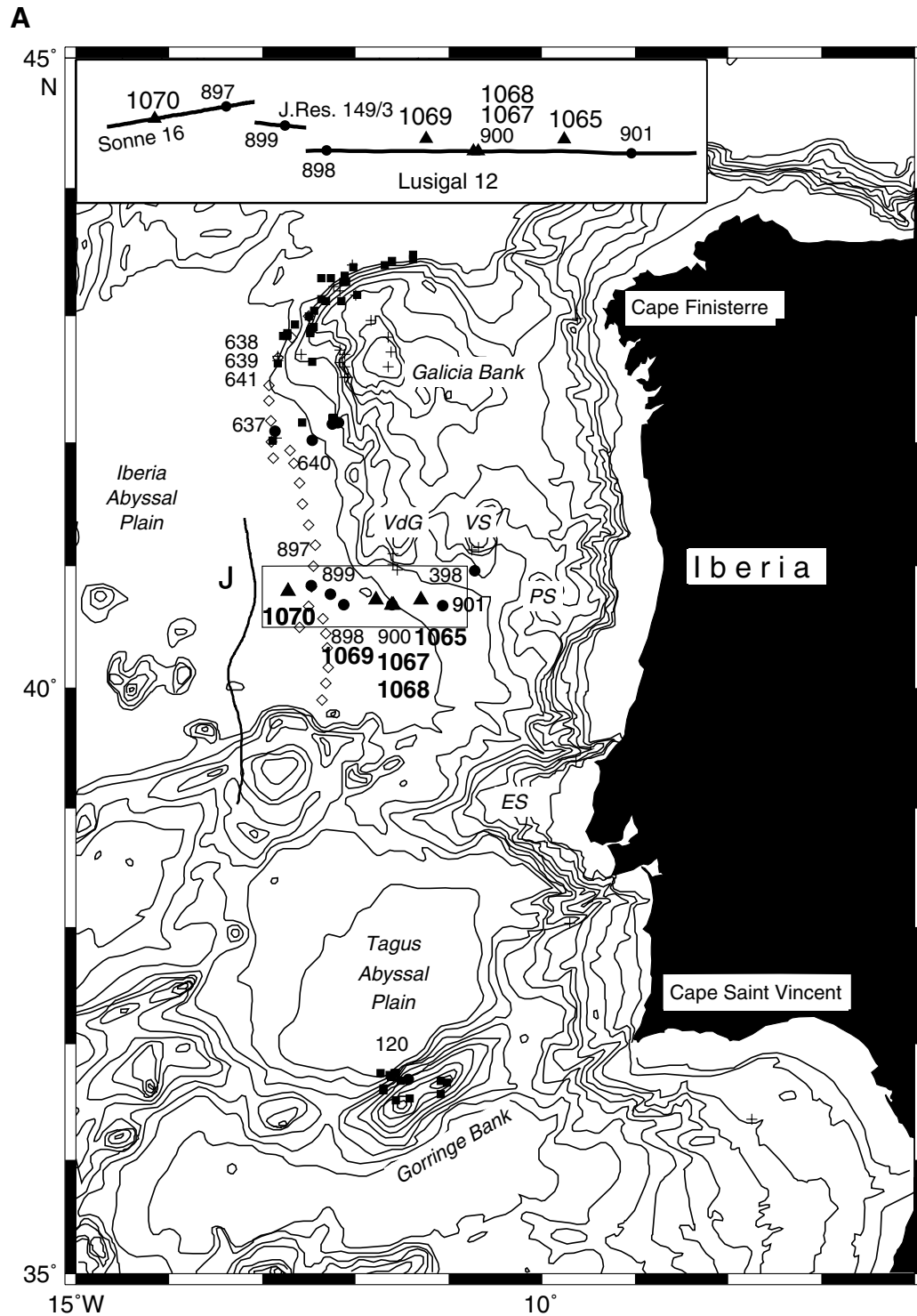
Figure F1 (continued). B. Composite west to east (left to right) cross section through the Leg 149 and Leg 173 drill sites along the tracks shown in Figure F1A (inset), p. 15. Site in parentheses are offset a short distance from the profile. Depths and extents of patterns are diagrammatic. Solid circles = gabbro and amphibolite, + = peridotite, ? = uncertain identification. VE = vertical exaggeration.
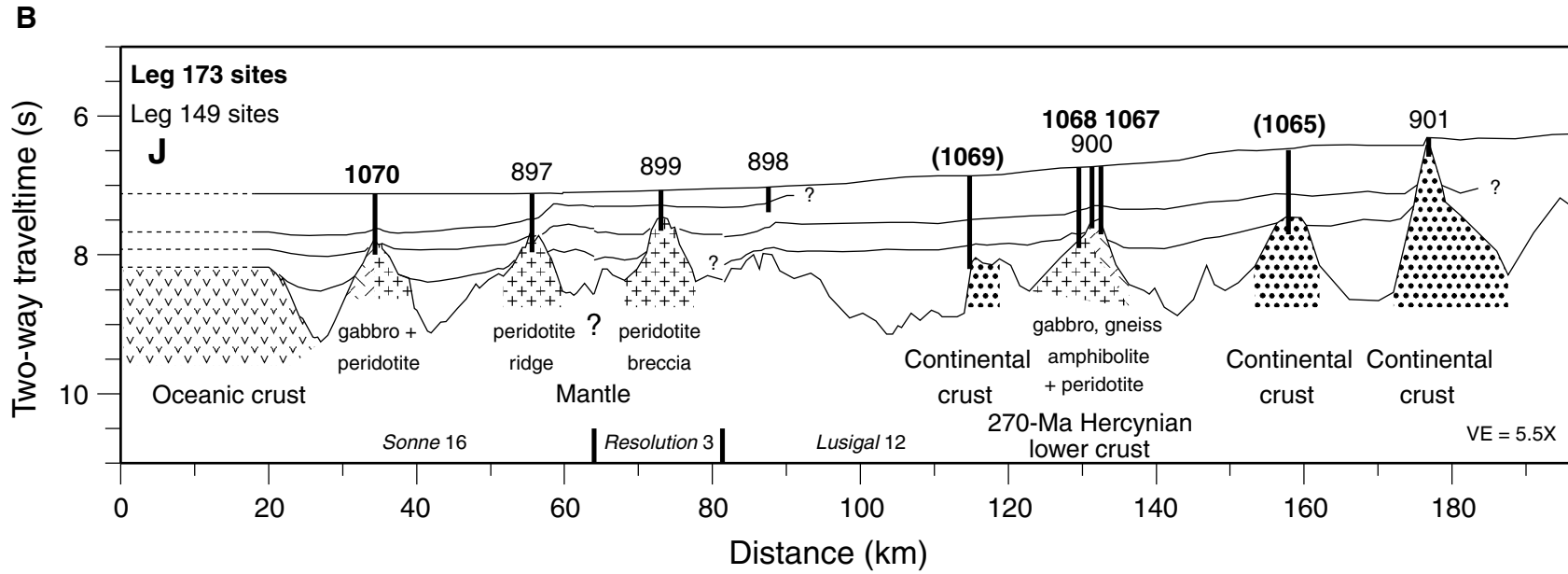
Figure F2. Plot of remanent intensity (**A**) before and (**B**) after 60-mT AF demagnetization and (**C**) volume magnetic susceptibility all as a function of sub-bottom depth in Hole 1070A. Upon demagnetization to 60 mT, a significant decrease in intensity and a shift of inclination toward negative values were observed, suggesting that drilling-induced magnetization is present. Horizontal axes are log scales.
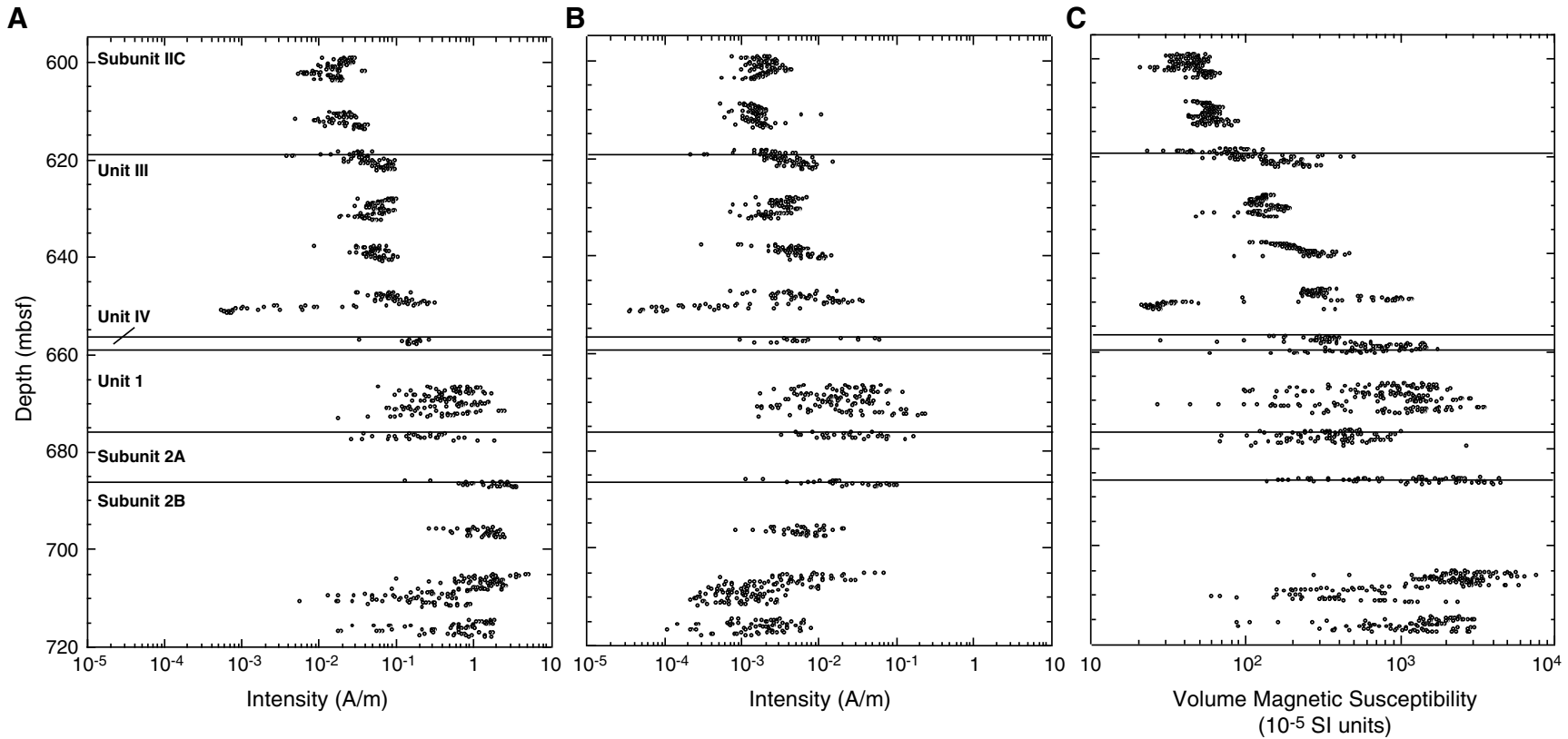
Figure F3. Downhole variation of magnetic inclination (**A**) before and (**B**) after AF demagnetization at 60 mT for Hole 1070A. Large squares = discrete samples taken from the center of the undisturbed parts of the working-half section. Parts of the recovered core had a significant amount of mechanical disturbance of the sediments; thus, AF demagnetization of the archive halves of cores was not always effective at removing the drilling induced overprint. Shaded area = the inferred magnetic polarity zone within the sepentinized peridotites.
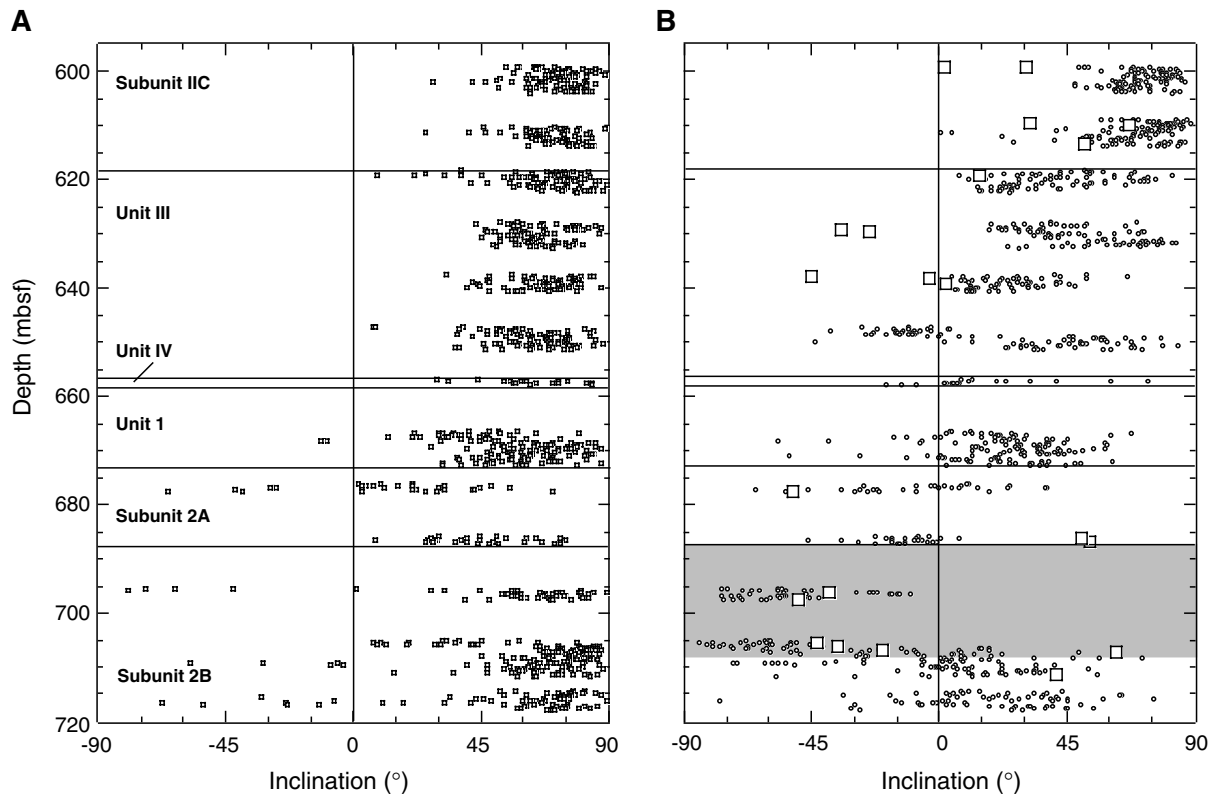
Figure F4. Representative vector end-point diagrams showing the results of (**A**) AF demagnetization for discrete Sample 173-1070A-4R-1, 113–115 cm, and (**B**) thermal demagnetization for Sample 173-1070A-4R-2, 2–4 cm (both samples are from Unit III). Solid circles = the projection of the magnetization vector end-points on the vertical plane. Crosses = the projection of the magnetization vector end-points on the horizontal plane. (Continued on next page.)
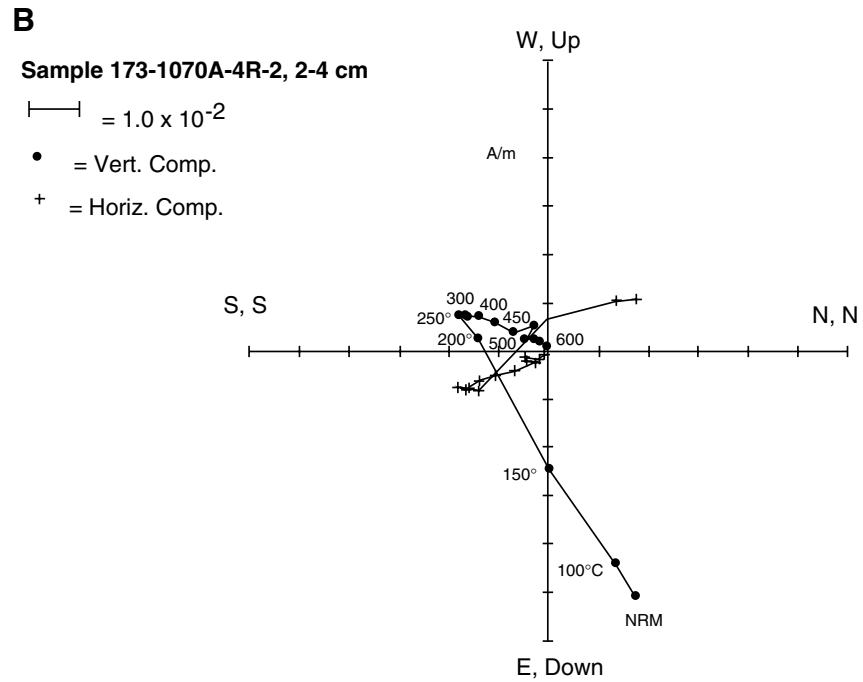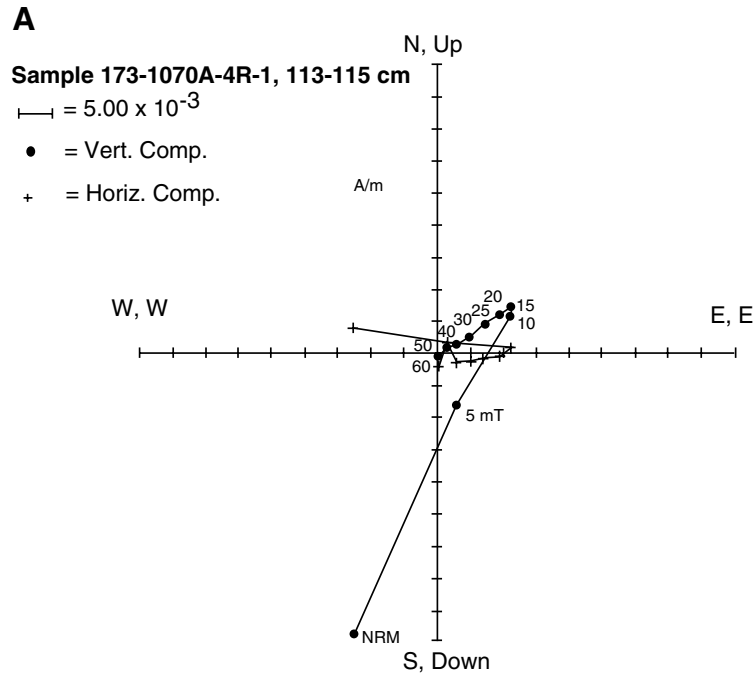
Figure F4 (continued). Representative vector end-point diagrams showing the results of thermal demagnetization for serpentinized peridotite in (**C**) Sample 173-1070A-10R-1, 72–74 cm, and (**D**) Sample 173-1070A-11R-2, 99–101 cm. Solid circles = the projection of the magnetization vector end-points on the vertical plane. Crosses = the projection of the magnetization vector end-points on the horizontal plane.
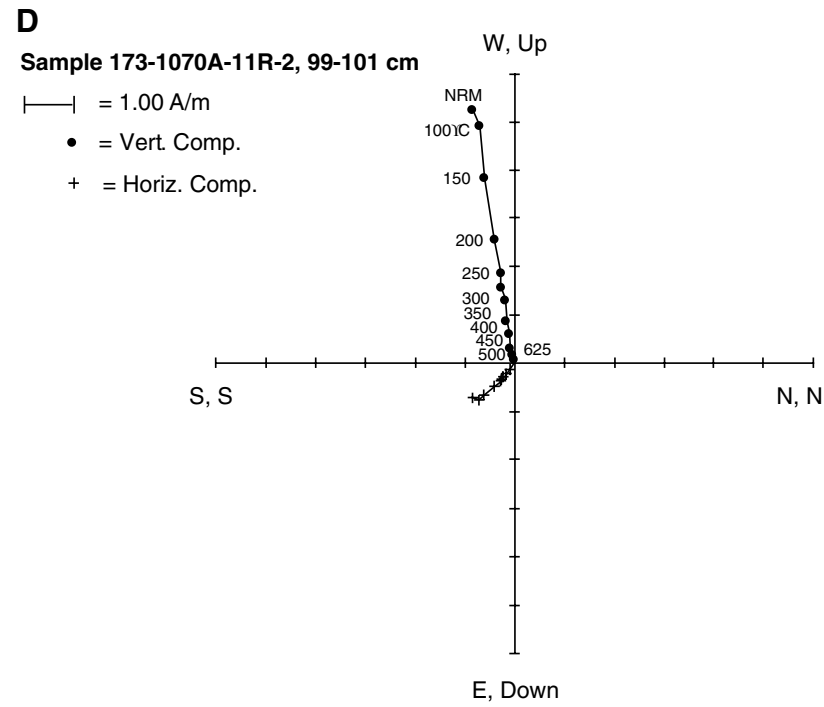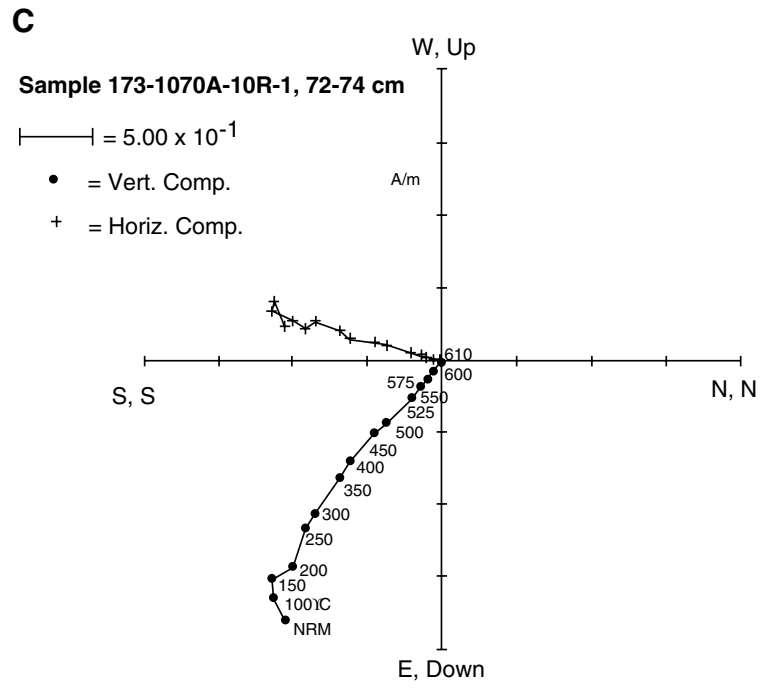
Figure F5. Representative vector end-point diagrams showing the results of (**A**) AF demagnetization on the reversely magnetized Sample 173-1068A-7R-4, 86–88 cm, and (**B**) thermal demagnetization for discrete serpentinized peridotite Sample 173-1068A-29R-3, 75–77 cm. Viscous remanent magnetization component (VRM) and stable component of magnetization, both defined by the least-squares best-fitting method, are indicated. Crosses = the projection of the magnetization vector end-points on the horizontal plane. Open circles = the projection of the magnetization vector end-points on the vertical plane. D = declination, I = inclination.
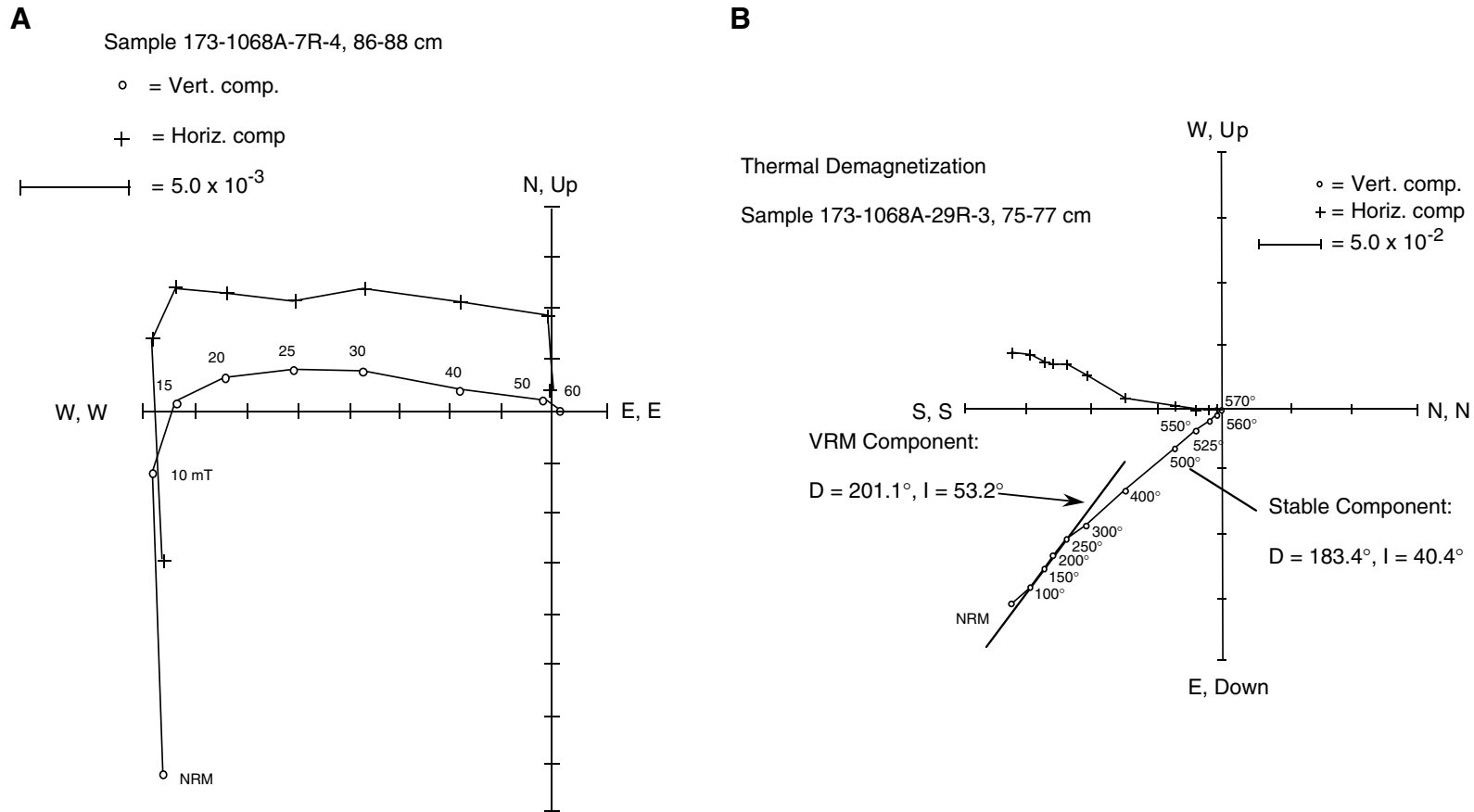
Figure F6. The hysteresis ratios plotted on a Day et al. (1977)-type diagram suggest that the bulk magnetic grain size is mainly in the pseudo–single domain (PSD) region. J_s = saturation magnetization, J_r = saturation remanent magnetization, H_c = coercivity, and H_{cr} = remanent coercive force. SD = single domain, MD = multidomain.
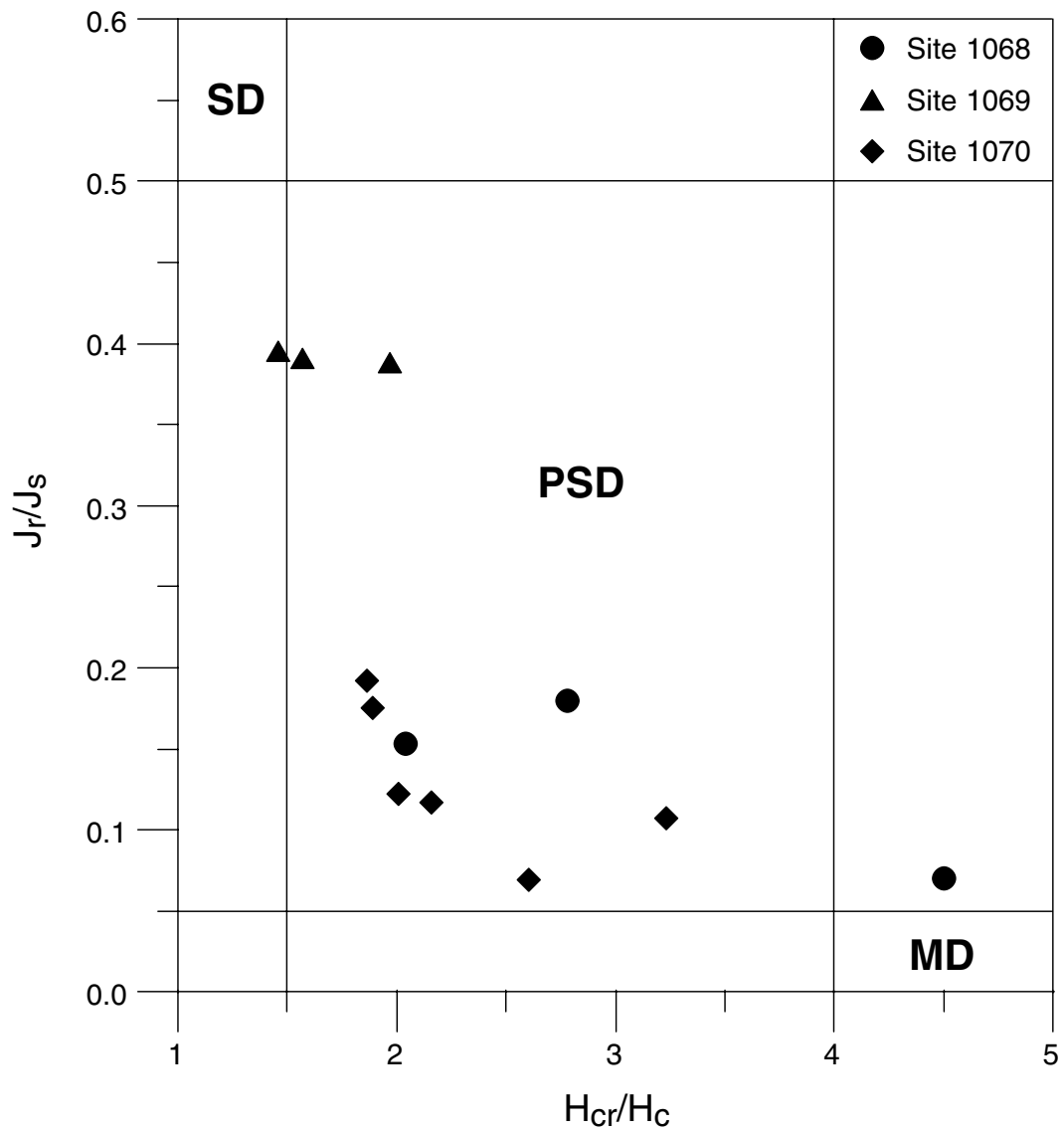
Figure F7. Low-temperature heating curves of saturation remanence normalized to 5 K ($SIRM_5$) for several representative samples. **A.** Altered peridotite sample (173-1070A-8R-1, 107–109 cm) from Site 1070. **B.** Fresher peridotite sample (173-1070A-14R-1, 21–23 cm) from Site 1070. (Continued on next page.)
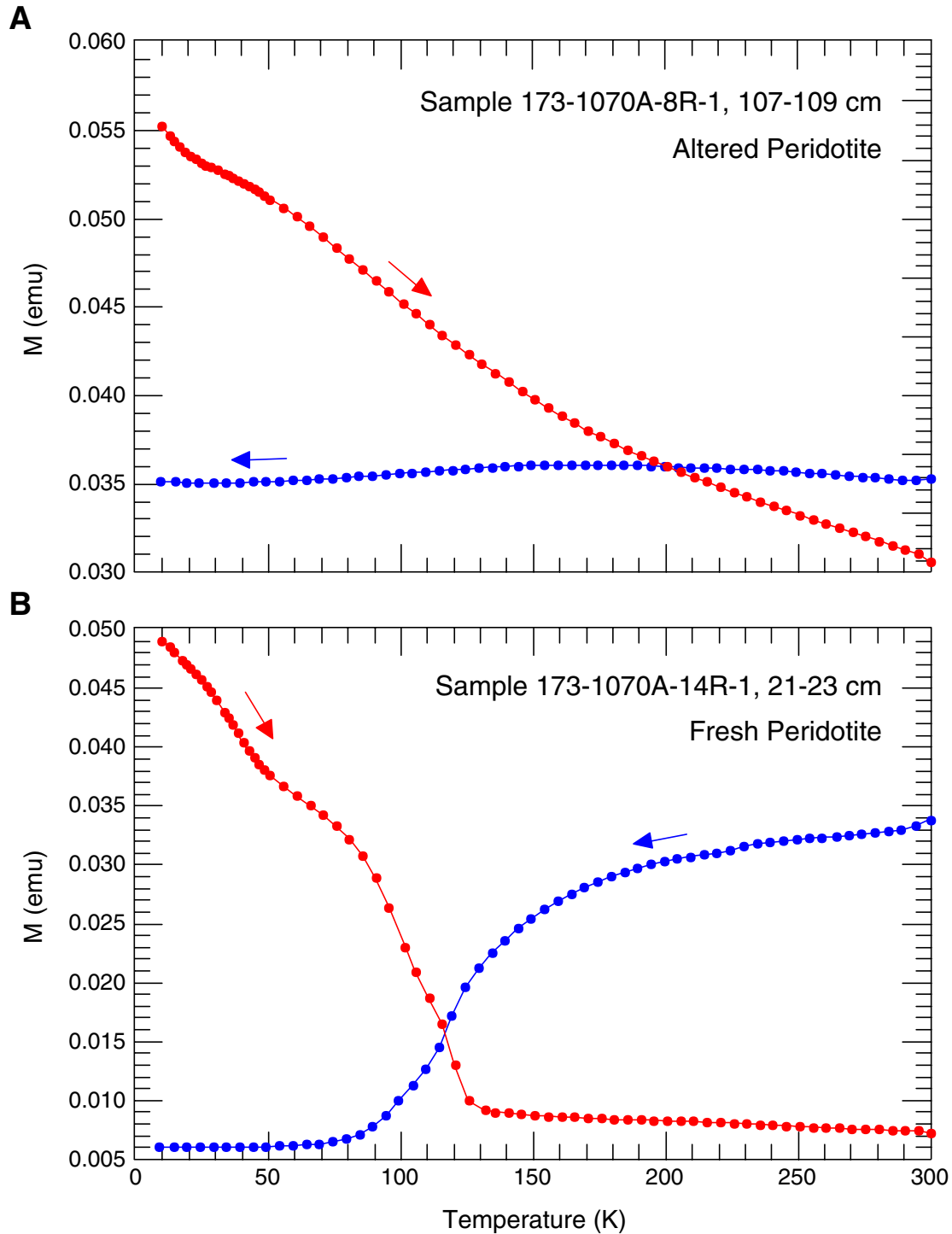
Figure F7 (continued). C. Amphibolite sample (173-1067A-22R-2, 12–14 cm) from Site 1067. **D.** Awaruite sample (173-1068A-26R-4, 18–20 cm) from Site 1068.
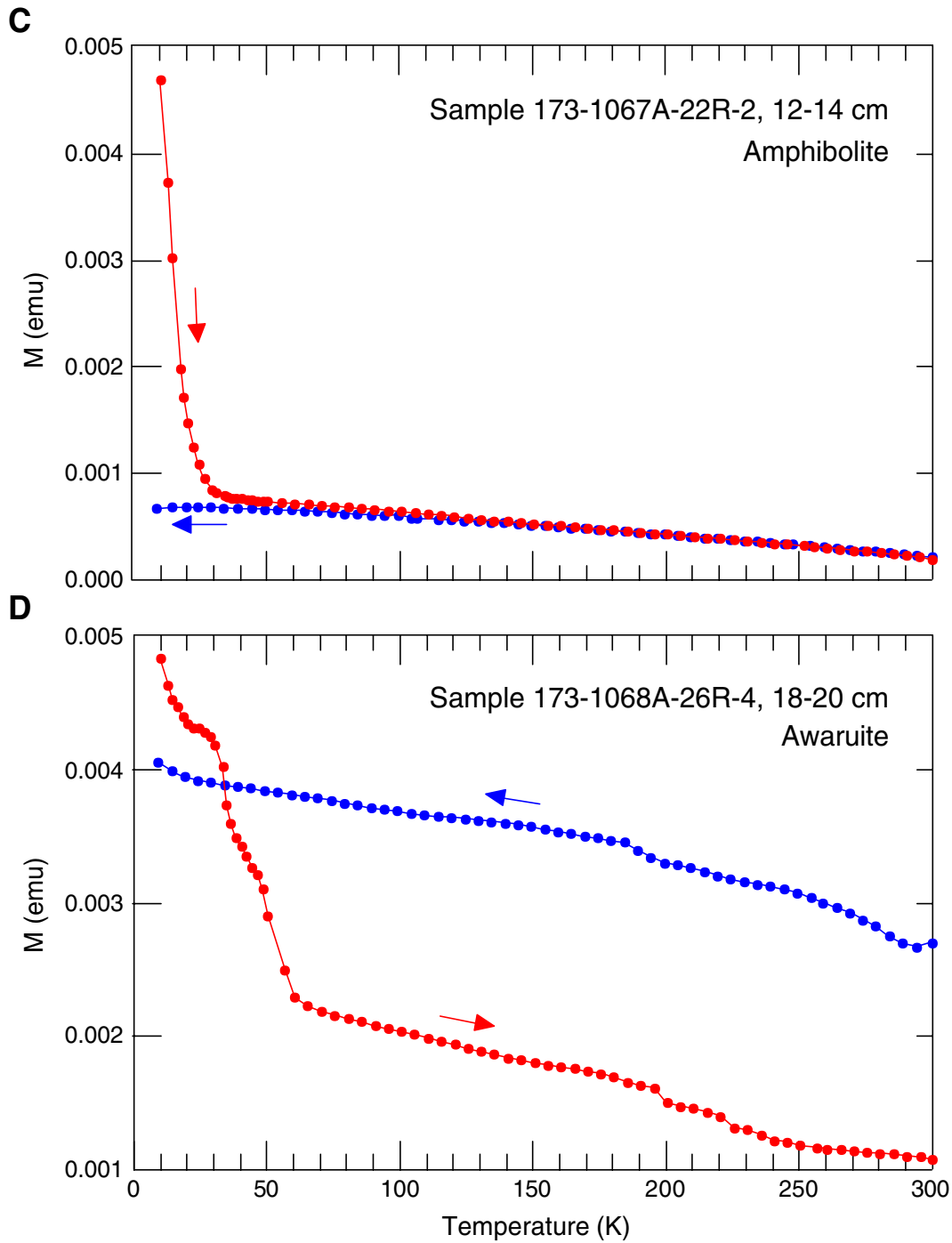
Figure F8. Typical thermomagnetic curves for Leg 173 peridotites. **A.** Altered peridotite sample (173-1070A-8R-1, 107–109 cm) from Site 1070. **B.** Fresher peridotite sample (173-1070A-11R-1, 81–83 cm) from Site 1070.
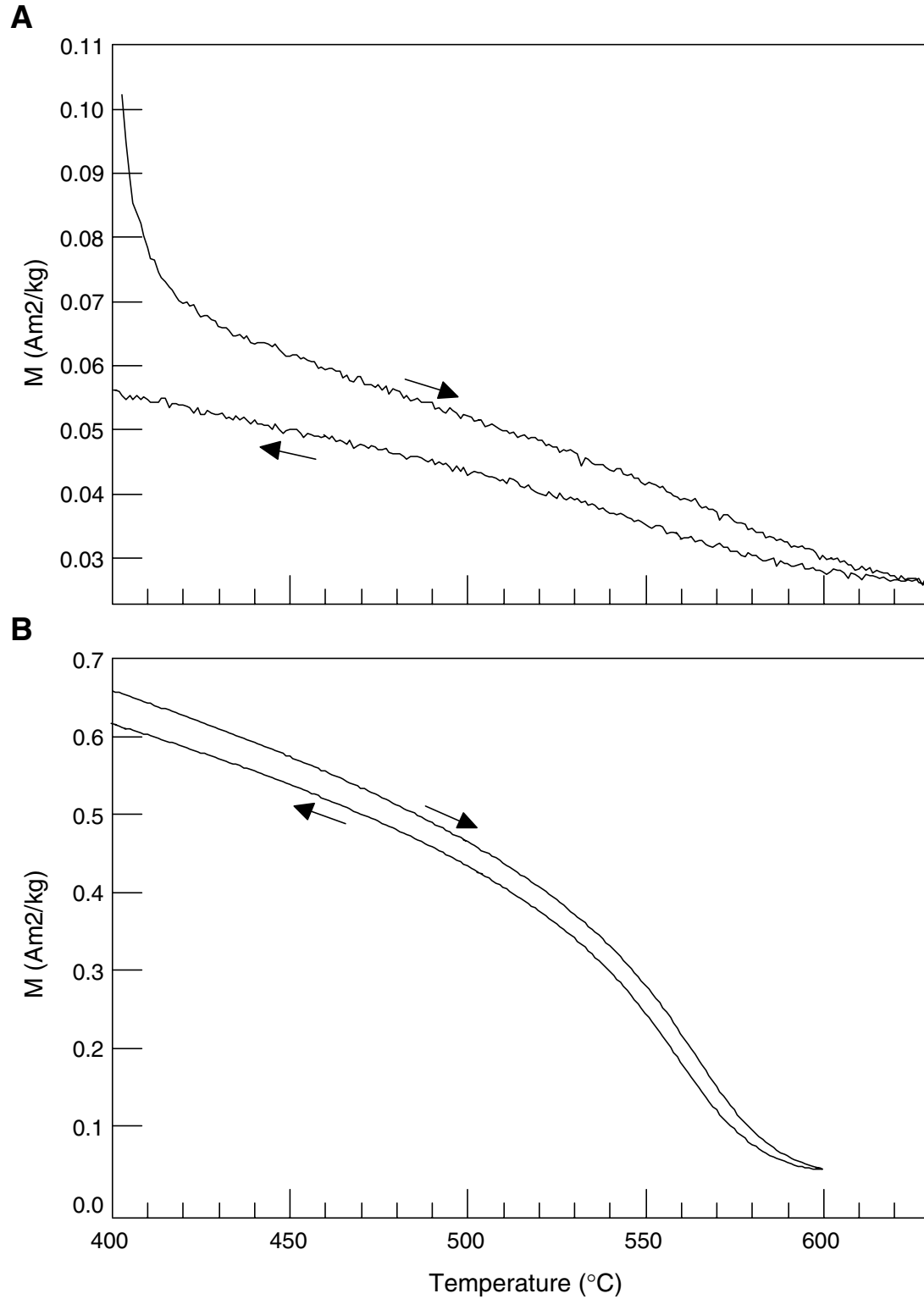
Figure F9. Representative diagram showing the temperature dependence of mass susceptibility for an altered peridotite sample (173-1070A-8R-1, 107–109 cm) from Site 1070 during warming from 15 to 300 K. **A.** In-phase (k') susceptibility measured at two different frequencies (95 and 1000 Hz) with two field amplitudes (100 and 1000 A/m). **B.** Quadrature (k'') susceptibility measured at two different frequencies (95 and 1000 Hz) with two field amplitudes (100 and 1000 A/m). The anomaly near 60 K shows both field dependence susceptibility and a peak in quadrature susceptibility.
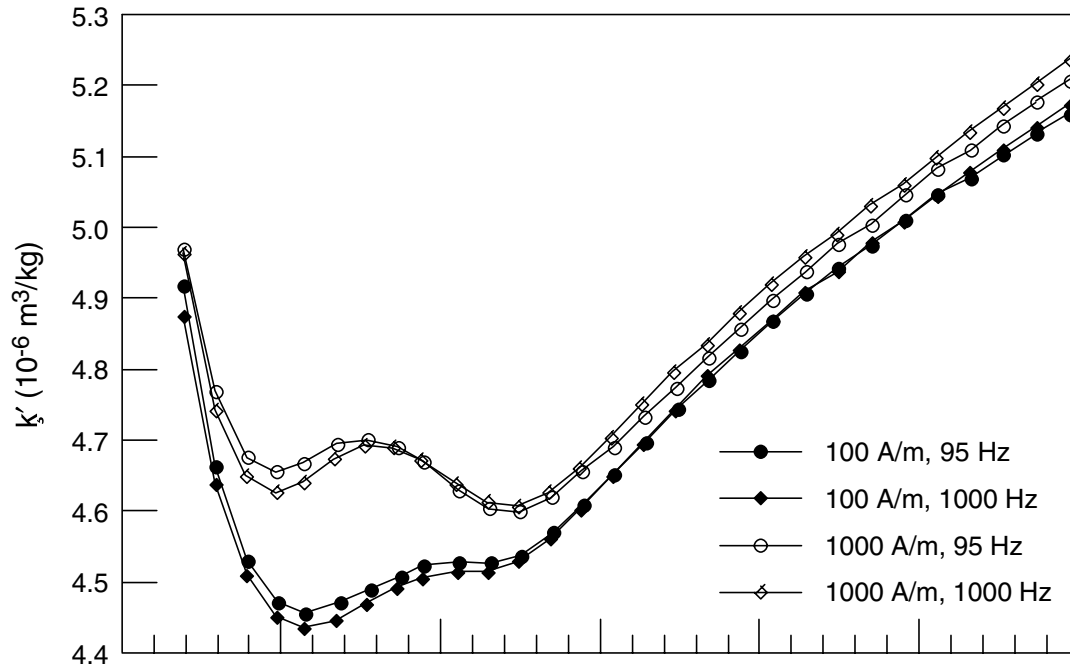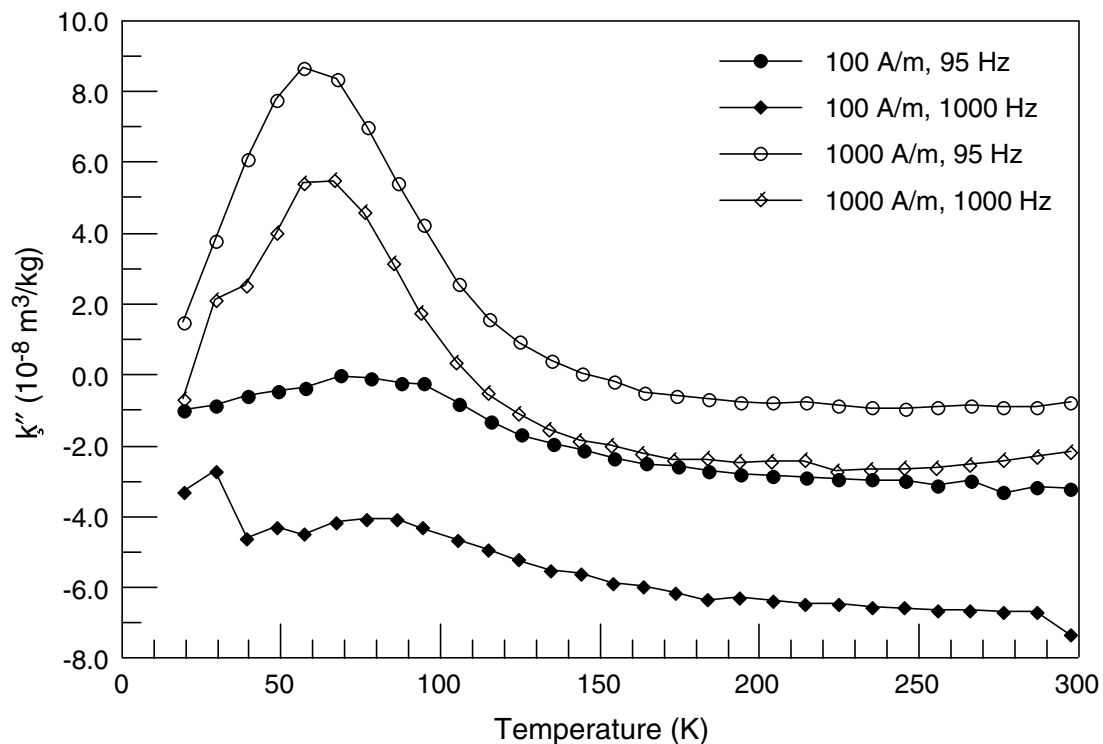
Table T1. Remanent magnetic properties of minicore samples from Leg 173 sites. (See table notes. Continued on next five pages).

Core, section, interval (cm)	Depth (mbsf)	Lithology	NRM (A/m)	NRM-Inc (°)	ChRM-Inc (°)	χ (10^{-5} SI)	Q ratio	MDF/(T_b) (mT)/(°C)	Polarity
173-1065A-									
1R-1, 38-40	251.38	Chalk	1.14E–4	–49.9	–57.7	3.4	0.09	30	R
1R-1, 107-109	252.07	Chalk	1.10E–4	–80.1	–18.8	0.2	1.53	50	R
1R-2, 18-20	252.68	Chalk	2.88E–5	–18.5	39.3	1.8	0.04	(200)	N
1R-2, 62-64	253.12	Chalk	2.83E–4	–42.4	–52.8	2.6	0.30	25	R
2R-1, 36-38	261.06	Chalk	7.08E–5	38.4	–31.5	6.0	0.03	(450)	R
2R-1, 137-139	262.07	Chalk	1.02E–4	32.0	59.8	4.6	0.06	(100)	N
3R-2, 11-13	271.91	Chalk	4.46E–5	52.3	–18.6	6.4	0.02	(450)	R
4R-1, 135-137	281.35	Chalk	3.49E–5	44.8	–37.5	1.2	0.08	20	R
4R-2, 53-55	282.03	Chalk	3.32E–5	44.2	–18.8	3.2	0.03	(300)	R
4R-2, 93-95	282.43	Chalk	9.05E–5	5.5	–20.0	1.8	0.14	30	R
5R-1, 47-49	290.07	Claystone	8.83E–5	58.5	–62.8	3.2	0.08	40	R
6R-1, 49-51	299.69	Chalk	6.45E–5	–36.5	–35.8	2.8	0.06	40	R
6R-1, 94-96	300.14	Chalk	1.18E–4	80.1	24.5	6.4	0.05	(300)	N
9R-1, 20-22	328.30	Siltstone	2.27E–4	–26.4	–34.4	35.0	0.02	40	R
9R-1, 48-50	328.58	Siltstone	3.10E–4	63.4	60.8	19.8	0.04	40	N
10R-CC, 24-26	337.94	Clay	1.90E–4	38.8	6.2	—	—	65	N?
14R-CC, 10-12	376.10	Clay	2.42E–4	45.0	–59.3	—	—	40	R?
14R-CC, 12-14	376.12	Clay	1.10E–3	43.1	–9.1	—	—	10	R?
16R-CC, 19-21	395.49	Clay	1.70E–4	32.2	–10.7	—	—	40	R?
17R-1, 15-17	405.05	Clay	3.77E–4	27.6	39.1	—	—	10	N
18R-1, 13-15	424.33	Clay	3.50E–4	47.3	59.9	—	—	10	N
18R-1, 35-37	424.55	Clay	3.40E–4	8.1	53.6	28.2	0.03	25	N
18R-CC, 5-7	424.68	Clay	4.51E–4	9.92	15.7	—	—	40	N
23R-CC, 5-7	502.14	Claystone	5.09E–5	55.2	71.1	—	—	(350)	N
24R-1,43-45	521.20	Claystone	1.98E–4	57.0	39.2	—	—	(250)	N
26R-1, 23-25	540.23	Claystone	2.28E–4	45.9	51.3	19.2	0.03	(350)	N
27R-1, 24-26	549.94	Claystone	1.84E–4	32.9	19.2	28.6	0.02	(300)	N
27R-1, 40-42	550.10	Claystone	1.67E–4	41.7	28.2	29.6	0.02	(275)	N
27R-1, 59-61	550.29	Claystone	1.36E–4	41.3	25.9	30.4	0.01	(200)	N
27R-1, 70-72	550.4	Claystone	2.02E–4	24.1	37.4	28.6	0.02	(200)	N
27R-1, 89-91	550.59	Claystone	1.83E–4	25.1	26.4	28.2	0.02	(225)	N
27R-1, 103-105	550.73	Claystone	4.64E–5	45.1	59.0	29.2	0.004	(350)	N
27R-1, 117-119	550.87	Claystone	1.39E–4	8.9	22.0	27.2	0.01	(250)	N
27R-2, 5-7	551.25	Claystone	1.22E–4	23.4	39.1	28.8	0.01	(270)	N
27R-2, 33-35	551.53	Claystone	3.19E–4	27.9	27.7	34.4	0.03	(225)	N
27R-2, 45-47	551.65	Claystone	2.24E–4	10.3	3.1	29.6	0.02	(300)	N
27R-2, 51-53	551.71	Claystone	1.50E–4	55.7	43.7	29.4	0.01	(200)	N
27R-2, 57-59	551.77	Claystone	9.85E–5	19.0	29.9	29.4	0.01	(275)	N
27R-2, 73-75	551.93	Claystone	1.40E–4	27.6	26.7	25.4	0.01	(325)	N
27R-2, 115-117	552.35	Claystone	1.54E–4	20.5	3.6	28.6	0.02	(300)	N
28R-1, 74-76	560.04	Claystone	4.38E–4	69.3	58.0	24.6	0.05	(250)	N
29R-1, 38-40	569.28	Claystone	1.87E–4	–24.0	–30.6	—	—	(350)	R
29R-1, 98-100	569.88	Claystone	3.24E–4	3.1	8.5	—	—	(320)	N
29R-CC, 6-8	570.12	Claystone	3.15E–4	–24.8	–36.8	—	—	(350)	R
30R-1, 76-78	579.26	Claystone	1.29E–4	24.9	18.5	—	—	(280)	N
31R-1, 60-62	588.7	Claystone	1.57E–4	0.3	–39.4	—	—	(350)	R
31R-1, 119-121	589.29	Claystone	1.97E–4	5.3	1.6	—	—	(325)	N?
32R-1, 100-102	598.7	Claystone	1.80E–4	–33.1	–52.0	—	—	(350)	R
32R-1, 111-113	598.81	Claystone	1.67E–4	–20.0	–46.5	—	—	(320)	R
33R-1, 15-17	607.55	Claystone	1.80E–4	31.4	30.5	21.2	0.02	(350)	N
33R-2, 19-21	609.04	Claystone	1.82E–4	10.5	11.3	27.0	0.02	(280)	N
34R-1, 8-10	617.18	Claystone	1.93E–4	–5.9	–39.1	29.0	0.02	(350)	R
173-1067A-									
1R-2, 89-91	650.39	Claystone	1.67E–4	62.6	68.5	12.9	0.04	(270)	N
2R-3, 50-52	661.10	Claystone	1.03E–4	43.1	–48.7	18.8	0.12	(400)	R
3R-3, 100-102	671.30	Claystone	1.93E–4	89.7	79.1	27.4	0.03	(400)	N
4R-2, 61-63	679.01	Claystone	9.89E–5	58.8	42.2	16.8	0.02	30	N
4R-2, 73-75	679.13	Claystone	1.16E–4	81.0	35.8	21.9	0.01	(400)	N
5R-1, 53-55	687.03	Claystone	9.03E–5	66.5	63.4	11.8	0.02	20	N
5R-2, 86-88	688.86	Claystone	7.49E–3	34.5	16.7	41.3	0.64	(250)	N
5R-3, 49-51	690.11	Claystone	1.37E–3	81.0	–17.7	14.0	0.27	15	R
6R-1, 57-59	696.67	Claystone	7.43E–4	46.2	27.5	14.6	0.14	45	N
6R-2, 14-16	697.74	Claystone	1.77E–4	59.2	31.5	6.6	0.07	45	N
8R-1, 136-138	716.86	Claystone	1.11E–4	64.3	24.2	2.4	0.13	15	N
8R-3, 115-117	719.65	Claystone	9.65E–5	39.4	27.1	14.2	0.02	20	N
9R-1, 68-70	725.88	Claystone	2.72E–3	67.2	63.9	19.6	0.39	35	N

Table T1 (continued).

Core, section, interval (cm)	Depth (mbsf)	Lithology	NRM (A/m)	NRM-Inc (°)	ChRM-Inc (°)	χ (10^{-5} SI)	Q ratio	MDF/(T_b) (mT)/(°C)	Polarity
10R-1, 113-115	735.93	Claystone	5.76E–3	–35.7	–49.5	23.8	0.68	25	R
10R-1, 122-124	736.02	Claystone	1.39E–2	62.0	28.9	24.2	1.60	10	N
10R-2, 58-60	736.88	Claystone	2.07E–3	20.4	–6.2	22.8	0.25	40	N?
10R-3, 38-40	738.18	Claystone	1.56E–3	–2.3	–3.1	18.0	0.24	100	N?
10R-4, 36-38	739.16	Claystone	1.93E–3	47.2	38.0	21.2	0.25	60	N
11R-1, 39-41	739.99	Claystone	8.60E–4	–31.7	0.2	21.6	0.11	80	N?
11R-1, 89-91	740.49	Claystone	5.94E–3	45.1	5.3	27.8	0.60	30	N
11R-2, 25-27	741.35	Claystone	1.25E–2	–35.0	–33.5	32.6	1.07	40	R
11R-3, 26-28	742.86	Claystone	3.23E–3	–2.4	–1.9	19.6	0.46	100	R?
11R-3, 61-63	743.21	Claystone	1.46E–3	69.4	48.1	20.6	0.20	20	N
12R-1, 8-10	744.58	Claystone	2.85E–2	9.1	–25.2	39.6	2.01	40	R
12R-1, 33-35	744.83	Claystone	3.85E–2	63.9	56.3	87.8	1.22	15	N
12R-2, 25-27	745.75	Claystone	2.10E–2	69.9	26.5	39.2	1.50	25	N
12R-2, 43-45	745.93	Claystone	4.52E–2	–3.7	–4.0	55.4	2.28	40	N?
16R-1, 49-51	764.30	Amphibolite	3.95E–2	79.9	68.4	98.5	1.12	(570)	N
16R-1, 83-85	764.64	Amphibolite	4.36E–2	53.6	57.7	—	—	70	N
16R-2, 9-11	784.22	Amphibolite	5.31E–2	50.7	55.5	86.2	1.72	(560)	N
16R-2, 13-15	784.26	Amphibolite	3.69E–2	32.8	33.1	—	—	70	N
18R-2, 28-30	803.43	Amphibolite	2.38E–2	86.9	88.0	89.1	0.75	(560)	N
18R-2, 77-79	803.92	Amphibolite	2.34E–2	72.6	70.5	81.4	0.80	(570)	N
18R-2, 87-89	804.02	Amphibolite	1.44E–2	53.7	13.7	—	—	70	N
19R-2, 28-30	813.2	Breccia	1.05E–2	14.9	13.1	75.1	0.39	(565)	N
20R-1, 100-102	822.10	Breccia	5.20E–2	–17.9	–9.6	91.9	1.58	(570)	R
21R-1, 114-116	831.94	Amphibolite	2.51E–3	58.1	71.1	64.2	0.01	(570)	N
22R-1, 29-31	840.69	Amphibolite	1.57E–3	48.9	39.5	76.0	0.06	(575)	N
23R-3, 4-6	852.89	Metagabbro	3.40E–3	50.5	43.8	127.7	0.09	(500)	N
173-1068A-									
1R-1, 51-53	711.81	Claystone	1.36E–2	47.8	29.3	40.2	0.94	30	N
1R-1, 59-61	711.88	Claystone	9.98E–4	58.9	67.2	22.2	0.13	15	N
1R-1, 76-78	712.06	Claystone	2.55E–4	–26.4	–32.2	14.4	0.05	40	R
1R-2, 129-131	714.09	Claystone	2.57E–4	–21.1	–20.3	15.4	0.05	20	R
1R-3, 19-21	714.49	Claystone	3.24E–4	–14.7	–23.2	17.6	0.05	50	R
1R-4, 116-118	716.96	Claystone	8.99E–5	10.2	–9.3	10.2	0.02	20	R
1R-5, 103-105	718.33	Claystone	1.23E–4	–14.0	–28.7	14.6	0.02	55	R
1R-6, 38-40	719.18	Claystone	1.06E–4	59.1	63.0	18.0	0.02	20	N
2R-1, 13-15	721.03	Claystone	5.01E–4	28.6	64.5	22.5	0.06	15	N
2R-1, 19-21	721.09	Claystone	4.22E–4	–10.6	66.5	19.7	0.06	15	N
2R-1, 23-25	721.13	Claystone	1.44E–4	27.8	61.2	5.3	0.08	20	N
2R-1, 58-60	721.48	Claystone	8.81E–5	36.1	34.9	16.8	0.01	40	N
2R-2, 74-76	723.14	Claystone	6.88E–4	–34.6	–40.0	15.0	0.13	45	R
2R-3, 85-87	724.75	Claystone	5.95E–5	24.2	19.1	16.8	0.01	10	N
2R-4, 72-74	726.12	Claystone	7.70E–5	–13.0	–8.7	14.8	0.01	20	R
2R-5, 38-40	727.28	Claystone	4.83E–5	15.1	18.3	14.6	0.01	20	N
3R-2, 139-141	732.99	Claystone	1.44E–4	44.1	47.0	19.4	0.02	(500)	N
3R-4, 12-14	734.72	Claystone	1.11E–4	56.3	50.6	19.9	0.02	(500)	N
3R-5, 28-30	736.38	Claystone	7.40E–5	25.8	9.4	20.4	0.01	30	N
3R-6, 8-10	737.68	Claystone	1.12E–3	35.8	31.7	22.9	0.14	(400)	N
3R-6, 87-89	738.47	Claystone	1.01E–4	–3.7	–41.9	17.3	0.02	(300)	R
3R-7, 0-2	739.10	Claystone	6.98E–5	48.9	—	16.4	0.01		
4R-1, 42-44	740.72	Claystone	1.34E–4	41.9	33.1	19.9	0.02	(200)	N
4R-2, 12-14	741.92	Claystone	1.68E–4	–73.0	–52.8	11.0	0.04	(300)	R
4R-3, 85-87	744.15	Claystone	1.96E–4	67.9	55.7	16.6	0.03	(200)	N
4R-4, 95-97	745.75	Claystone	7.63E–5	32.4	37.3	19.7	0.01	(300)	N
4R-5, 83-85	747.13	Claystone	5.91E–5	7.7	—	22.7	0.01		
4R-6, 2-4	747.82	Claystone	7.65E–5	51.5	22.7	21.7	0.01	(150)	N
4R-6, 69-71	748.49	Claystone	1.36E–3	55.0	–27.0	32.5	0.12	(300)	R
5R-1, 47-49	750.37	Claystone	1.21E–2	40.1	49.9	42.9	0.79	(400)	N
5R-2, 98-100	752.38	Claystone	4.86E–2	76.3	72.6	40.6	3.34	(200)	N
5R-3, 25-27	753.15	Claystone	2.43E–2	34.5	19.8	62.1	1.09	(200)	N
5R-4, 86-88	755.26	Claystone	2.82E–3	–5.9	—	30.4	0.26		
5R-5, 62-64	756.52	Claystone	1.92E–2	44.0	33.9	43.7	1.23	(300)	N
5R-6, 64-66	757.54	Claystone	1.05E–2	36.8	23.3	29.2	1.00	(200)	N
6R-1, 108-110	760.68	Claystone	1.33E–5	35.6	40.7	32.8	0.001	20	N
6R-2, 126-128	762.36	Claystone	4.76E–5	–25.8	–63.5	14.4	0.01	20	R
6R-3, 43-45	763.03	Claystone	3.37E–5	–6.7	—	14.4	0.01		
6R-3, 62-64	763.22	Claystone	1.90E–4	49.2	19.4	12.6	0.04	25	N
6R-3, 108-110	763.68	Claystone	2.41E–4	69.1	47.9	12.4	0.05	30	N
6R-3, 137-139	763.97	Claystone	9.60E–4	49.1	—	6.0	0.45		
6R-4, 60-62	764.70	Claystone	2.09E–2	35.6	42.5	58.6	0.99	20	N

Table T1 (continued).

Core, section, interval (cm)	Depth (mbsf)	Lithology	NRM (A/m)	NRM-Inc (°)	ChRM-Inc (°)	χ (10^{-5} SI)	Q ratio	MDF/(T_b) (mT)/(°C)	Polarity
6R-5, 32-34	765.92	Claystone	1.69E–2	–7.0	–41.0	49.0	0.96	20	R
6R-6, 126-128	768.36	Claystone	6.47E–4	13.1	–4.8	13.6	0.13	10	R
6R-7, 36-38	768.96	Claystone	5.25E–3	–6.4	19.0	25.6	0.51	(350)	N
7R-1, 34-36	769.64	Claystone	8.59E–3	–20.0	–18.7	28.8	0.83	10	R
7R-2, 120-122	772.00	Claystone	4.68E–2	4.8	–62.0	85.4	1.53	10	R
7R-3, 96-98	773.26	Claystone	1.01E–2	34.2	35.6	27.8	1.01	10	N
7R-4, 18-20	773.98	Claystone	8.91E–3	–16.1	–61.2	39.6	0.63	15	R
7R-4, 23-25	774.03	Claystone	1.62E–2	–13.7	–15.2	26.8	1.69	10	R
7R-4, 32-34	774.12	Claystone	5.26E–2	26.8	–12.3	55.6	2.64	10	R
7R-4, 51-53	774.31	Claystone	3.01E–2	–11.0	–14.5	35.6	2.36	20	R
7R-4, 72-74	774.52	Claystone	2.04E–3	–5.3	—	8.2	0.69		
7R-4, 86-88	774.66	Claystone	7.86E–2	74.2	65.2	572.7	0.38	25	N
7R-4, 124-126	775.04	Claystone	6.05E–2	–8.0	–52.6	62.4	2.71	40	R
7R-5, 9-11	775.39	Claystone	2.02E–2	–3.4	–31.0	47.6	1.18	50	R
7R-5, 64-66	775.94	Claystone	7.35E–2	62.0	69.1	—	—		
7R-5, 83-85	776.13	Claystone	5.11E–2	–1.9	–8.1	63.6	2.24	15	R
8R-1, 55-57	779.45	Claystone	7.67E–2	46.1	35.5	122.8	1.74	(200)	N
8R-1, 108-110	779.98	Claystone	9.54E–2	47.5	38.9	87.4	3.05	20	N
8R-2, 9-11	780.49	Claystone	2.51E–2	–8.5	–30.2	71.0	0.99	(300)	R
8R-2, 19-21	780.59	Claystone	4.66E–2	–4.7	–32.1	115.2	1.13	(300)	R
8R-2, 30-32	780.70	Claystone	1.05E–1	–54.0	35.5	115.8	2.53	10	R
8R-2, 43-45	780.83	Claystone	4.04E–2	–24.0	–43.0	98.4	1.15	10	R
8R-2, 72-74	781.12	Claystone	9.34E–2	49.5	37.0	145.4	1.79	(400)	N
8R-2, 101-103	781.41	Claystone	6.62E–2	–21.5	–22.6	67.4	2.74	(250)	R
8R-2, 143-145	781.83	Claystone	3.05E–2	33.4	35.9	65.6	1.30	10	N
8R-3, 112-114	783.02	Claystone	2.14E–2	79.4	–12.9	77.5	0.77	(400)	R
8R-4, 7-9	783.47	Claystone	3.92E–2	62.3	–46.8	75.9	1.44	(550)	R
8R-5, 95-97	785.85	Claystone	1.16E–3	74.2	–39.3	26.6	0.12	(400)	R
9R-2, 63-65	790.63	Claystone	3.72E–4	–5.2	11.1	11.8	0.09	(250)	N
9R-3, 65-67	792.15	Claystone	2.66E–4	23.6	43.8	13.4	0.06	(400)	N
9R-4, 49-51	793.49	Claystone	3.20E–3	–32.1	–21.2	10.6	0.84	60	R
9R-5, 11-13	794.61	Claystone	4.21E–4	–46.6	–65.4	10.4	0.11	60	R
9R-5, 53-55	795.03	Claystone	9.81E–4	49.9	31.6	18.4	0.15	30	N
9R-5, 67-69	795.17	Claystone	3.72E–4	88.0	73.8	10.6	0.10	25	N
9R-5, 87-89	795.37	Claystone	7.02E–4	63.8	54.5	7.4	0.26	25	N
9R-6, 141-143	797.41	Claystone	1.63E–4	–9.8	47.7	8.4	0.05	15	N
9R-7, 35-37	797.85	Claystone	2.06E–4	19.3	26.8	8.8	0.07	20	N
10R-1, 40-42	798.50	Chalk	5.25E–4	37.8	52.1	16.0	0.09	25	N
10R-1, 50-52	798.60	Chalk	1.12E–3	58.3	59.4	10.4	0.30	40	N
10R-1, 71-73	798.81	Chalk	2.16E–4	–12.7	–9.5	8.0	0.08	30	R
10R-2, 27-29	799.87	Chalk	1.91E–4	45.2	65.1	7.8	0.07	60	N
10R-2, 38-40	799.98	Chalk	2.05E–4	63.3	47.9	8.0	0.07	15	N
10R-3, 79-81	801.89	Chalk	1.67E–4	–16.9	–14.5	17.4	0.03	100	R
11R-1, 23-25	807.93	Claystone	4.05E–4	20.8	13.9	23.6	0.05	30	N
11R-2, 15-17	809.35	Claystone	1.81E–3	58.7	—	22.4	0.23		
11R-2, 26-28	809.46	Claystone	7.68E–4	63.4	59.0	11.2	0.19	20	N
11R-2, 74-76	809.94	Claystone	3.23E–4	–11.2	–20.6	10.6	0.09	25	R
11R-3, 77-79	811.47	Claystone	5.83E–4	71.8	22.2	13.0	0.13	(200)	N
11R-4, 13-15	812.33	Claystone	1.72E–3	4.3	–86.2	10.2	0.47	10	R?
11R-5, 94-96	814.64	Claystone	3.14E–3	–12.6	22.4	10.0	0.88	10	N
12R-1, 126-128	818.56	Claystone	9.99E–3	–16.5	–19.7	29.6	0.94	10	R
12R-2, 4-6	818.84	Claystone	1.64E–3	11.3	–6.6	25.8	0.18	10	R
12R-3, 108-110	821.38	Claystone	4.34E–2	30.7	54.6	113.0	1.07	40	N
12R-4, 78-80	822.58	Claystone	8.59E–2	–12.2	–5.2	110.2	2.18	15	R
12R-5, 67-69	823.97	Claystone	8.00E–2	10.8	–14.0	99.0	2.25	20	R
12R-6, 80-82	825.60	Claystone	6.73E–2	50.4	37.5	108.3	0.17	(200)	N
12R-7, 67-69	826.97	Claystone	1.33E–1	–36.5	–22.0	24.2	15.34	(400)	R
13R-1, 134-136	828.24	Claystone	1.14E–3	–16.3	67.9	32.2	0.10	10	N
13R-2, 147-149	829.87	Claystone	1.85E–3	6.7	57.4	17.2	0.30	(300)	N
13R-3, 148-150	831.38	Claystone	4.64E–3	25.8	22.3	20.4	0.63	10	N
13R-4, 7-9	831.47	Claystone	1.09E–2	12.6	–51.8	21.2	1.43	20	R
13R-4, 117-119	832.57	Claystone	1.41E–2	–4.7	–52.8	19.0	2.07	10	R
13R-5, 113-115	834.03	Claystone	1.48E–2	–1.6	18.4	41.6	0.99	20	N
13R-6, 11-13	834.51	Claystone	3.37E–2	4.1	67.2	51.0	1.84	(300)	N
13R-6, 52-54	834.92	Claystone	1.07E–3	85.5	68.3	28.2	0.11	25	N
13R-6, 60-62	835.00	Claystone	4.70E–4	27.1	28.7	10.8	0.12	10	N
13R-6, 68-70	835.08	Claystone	6.98E–4	33.4		13.2	0.15		
13R-6, 74-76	835.14	Claystone	6.65E–4	26.0	25.4	11.6	0.16	20	N
13R-6, 81-83	835.21	Claystone	7.93E–4	51.9	42.9	9.4	0.24	20	N

Table T1 (continued).

Core, section, interval (cm)	Depth (mbsf)	Lithology	NRM (A/m)	NRM-Inc (°)	ChRM-Inc (°)	χ (10^{-5} SI)	Q ratio	MDF/(T_b) (mT)/(°C)	Polarity
13R-6, 84-86	835.24	Claystone	6.38E–4	30.5	48.7	14.0	0.13	20	N
13R-6, 90-92	835.30	Claystone	6.20E–4	–32.9	–37.5	11.6	0.15	20	R
14R-1, 12-14	836.72	Chalk	3.95E–3	23.1	–13.0	11.9	0.93	(250)	R
14R-1, 26-28	836.86	Chalk	3.12E–2	39.1	–22.5	14.0	6.22	(575)	R
14R-1, 48-50	837.08	Chalk	1.44E–2	15.6	43.3	4.2	9.57	(300)	N
14R-1, 57-59	837.17	Chalk	3.95E–4	–33.3	–44.0	0.7	1.57	(300)	R
14R-1, 67-69	837.27	Chalk	2.66E–2	–19.1	34.1	5.0	14.85	(400)	N
14R-1, 83-85	837.43	Chalk	2.47E–2	0.2	62.6	6.3	10.94	(300)	N
14R-1, 106-108	837.66	Chalk	3.04E–2	–1.8	–38.1	5.1	16.64	(300)	R
14R-1, 120-122	837.80	Chalk	1.53E–2	–8.2	–28.7	6.7	6.37	(350)	R
14R-1, 138-140	837.98	Chalk	7.53E–3	–38.5	46.5	5.6	3.75	(475)	N
14R-2, 14-16	838.24	Chalk	1.17E–2	12.7	20.2	45.0	0.73	20	N
14R-2, 54-56	838.64	Chalk	1.44E–2	–40.5	–48.3	31.2	1.29	30	R
14R-2, 81-83	838.91	Chalk	7.29E–2	47.6	14.8	137.1	1.48	(300)	N
14R-2, 107-109	839.17	Chalk	1.01E–2	18.1	29.3	21.0	1.34	25	N
14R-2, 107-109	839.17	Chalk	1.01E–2	18.1	29.3	21.0	1.34	25	N
14R-3, 82-84	840.42	Chalk	6.96E–2	38.3	22.4	75.5	2.57	(300)	N
14R-3, 104-106	840.64	Chalk	8.48E–3	–12.9	–23.8	25.4	0.93	20	R
14R-4, 14-16	841.24	Chalk	9.61E–3	–9.7	–8.6	24.6	1.09	20	R
14R-4, 40-42	841.50	Chalk	1.76E–2	29.8	32.8	34.8	1.41	20	N
14R-4, 82-84	841.92	Chalk	5.26E–2	6.5	–20.6	254.4	0.58	(500)	R
14R-4, 125-127	842.35	Chalk	5.30E–3	–17.3	–19.3	25.4	0.58	80	R
14R-5, 9-11	842.69	Chalk	1.88E–2	64.8	–40.6	94.1	0.56	(300)	R
14R-5, 77-79	843.37	Chalk	4.26E–3	61.9	57.2	22.4	0.53	80	N
14R-6, 50-52	844.60	Chalk	4.99E–3	45.5	46.7	17.2	0.81	35	N
15R-1, 66-68	846.96	Chalk	3.52E–3	1.8	51.4	17.0	0.58	(350)	N
15R-2, 73-75	848.53	Chalk	9.33E–4	–26.9	10.2	13.4	0.19	(350)	N
15R-3, 54-56	849.84	Chalk	1.24E–3	33.9	39.3	15.2	0.23	25	N
15R-3, 82-84	850.12	Chalk	6.96E–2	38.3	34.5	75.5	2.57	(200)	N
15R-4, 46-48	850.76	Chalk	4.10E–3	27.7	–65.5	28.4	0.40	20	R
16R-1, 38-40	856.28	Breccia	3.87E–2	67.1	67.9	138.3	0.78	(200)	N
16R-4, 45-47	860.30	Breccia	1.11E–2	47.1	45.8	603.4	0.05	(350)	N
22R-1, 86-88	905.06	Peridotite	5.72E–3	73.9	—	44.7	0.36		
23R-1, 41-43	914.21	Peridotite	4.73E–1	43.5	–33.5	597.0	2.21	35	R
23R-1, 81-83	914.61	Peridotite	8.56E–2	–11.8	–19.8	64.4	3.71	(500)	R
24R-1, 65-67	923.85	Peridotite	7.45E–2	67.7	32.4	184.0	1.13	(300)	N
24R-1, 92-94	924.12	Peridotite	5.23E–2	–45.6	–30.9	57.5	2.54	(500)	R
25R-1, 111-113	933.71	Peridotite	2.48E–2	63.5	52.0	111.7	0.62	(400)	N
25R-2, 36-38	934.46	Peridotite	3.31E–2	31.4	20.8	9.1	10.15	(400)	N
25R-2, 92-94	935.02	Peridotite	2.13E–1	37.3	33.6	69.4	8.56	60	N
25R-2, 109-110	935.19	Peridotite	1.14E–1	–6.8	–16.9	29.1	10.93	(500)	R
26R-1, 77-79	937.77	Peridotite	9.99E–3	49.7	41.5	43.2	0.65	(300)	N
26R-1, 107-109	938.07	Peridotite	1.62E–2	50.2	46.9	135.4	0.33	(300)	N
26R-1, 112-114	938.12	Peridotite	1.31E–1	53.9	52.0	132.4	2.76	50	N
26R-2, 13-15	938.50	Peridotite	1.47E–1	30.1	22.4	35.6	11.52	(375)	N
26R-2, 48-50	938.85	Peridotite	3.69E–1	15.8	13.7	16.8	61.3	(500)	N
26R-2, 66-68	939.03	Peridotite	8.79E–2	41.3	38.6	55.2	4.44	40	N
26R-2, 92-94	939.29	Peridotite	3.00E–2	45.5	39.5	50.8	1.65	(400)	N
26R-3, 62-64	940.37	Peridotite	1.21E–1	–22.1	–16.4	38.3	8.82	(400)	R
26R-4, 18-20	941.11	Peridotite	6.68E–2	–44.2	–35.7	25.2	7.4	(400)	R
28R-1, 61-63	947.01	Peridotite	8.88E–2	52.4	45.0	258.5	0.96	(500)	N
28R-1, 121-123	947.61	Peridotite	9.80E–2	53.4	48.9	169.6	1.61	(300)	N
28R-2, 56-58	948.41	Peridotite	1.22E–1	56.4	47.6	202.8	1.68	35	N
28R-2, 62-64	948.48	Peridotite	7.12E–2	58.9	40.6	165.9	11.97	(400)	N
28R-2, 86-88	948.72	Peridotite	9.42E–2	–31.3	–29.6	30.3	8.67	(525)	R
28R-3, 57-59	949.76	Peridotite	5.29E–2	5.9	–20.3	14.2	10.39	(525)	R
29R-3, 48-50	953.99	Peridotite	1.69E–1	46.7	46.9	216.5	2.18	(400)	N
29R-3, 75-77	954.26	Peridotite	2.28E–1	42.5	39.4	212.9	2.99	(300)	N
29R-3, 94-96	954.45	Peridotite	1.13E–1	50.7	41.3	225.4	1.40	30	N
173-1069A-									
2R-2, 116-118	730.44	Claystone	2.33E–3	42.9	30.5	18.6	0.35	(150)	N
2R-3, 22-24	731.00	Claystone	8.34E–4	53.5	–3.0	14.0	0.17	(300)	N?
2R-3, 36-38	731.14	Claystone	9.15E–4	62.7	63.0	18.2	0.04	70	N
2R-3, 40-42	731.19	Claystone	8.88E–5	45.9	—				
2R-3, 47-49	732.25	Claystone	1.39E–4	36.7	—				
3R-2, 66-68	740.26	Claystone	6.42E–4	13.4					
3R-2, 73-75	740.33	Claystone	6.70E–5	–55.3					
3R-2, 78-80	740.38	Claystone	9.33E–5	26.3	–13.7	7.6	0.03	70	R?
3R-3, 9-11	741.19	Claystone	4.61E–4	43.6	–15.5	6.7	0.19	(500)	R

Table T1 (continued).

Core, section, interval (cm)	Depth (mbsf)	Lithology	NRM (A/m)	NRM-Inc (°)	ChRM-Inc (°)	χ (10⁻⁵ SI)	Q ratio	MDF/(T_b) (mT)/(°C)	Polarity
4R-2, 40-42	749.60	Claystone	6.78E–4	58.4					
4R-2, 53-55	749.67	Claystone	8.92E–5	–62.3					
7R-1, 12-14	776.92	Claystone	3.52E–2	24.7	18.3	59.2	1.66	(300)N	N
7R-1, 23-25	777.03	Claystone	1.77E–2	34.8	—	148.4	0.33		
7R-1, 45-47	777.25	Claystone	3.99E–2	43.1	46.7	86.4	1.29	(200)	N
7R-1, 74-76	777.54	Claystone	3.90E–2	42.1	—	37.0	2.94		
7R-1, 82-84	777.62	Claystone	5.19E–2	44.0	57.4	37.4	3.87	(200)	N
7R-1, 100-102	777.80	Claystone	2.67E–2	42.5	60.7	31.2	2.39	(200)	N
7R-1, 144-146	778.24	Claystone	2.84E–2	55.8	48.0	38.2	2.07	(550)	N
7R-2, 19-21	778.49	Claystone	2.30E–2	41.9	—		29.2	2.20	
7R-2, 29-31	778.59	Claystone	2.58E–2	40.7	–40.9	50.0	1.44	(250)	R
7R-2, 95-97	779.25	Claystone	3.13E–2	–44.6	–21.6	50.2	1.74	(200)	R
7R-3, 60-62	780.40	Claystone	1.09E–2	–35.3	–45.4	32.4	0.94	(300)	R
7R-3, 76-78	780.56	Claystone	5.79E–4	30.4	—	28.6	0.06		
7R-3, 79-81	780.59	Claystone	8.58E–3	–21.7	–60.8	31.8	0.75	(100)	R
7R-3, 107-109	780.87	Claystone	1.96E–2	–21.0	–50.3	28.2	1.94	(500)	R
8R-1, 110-112	787.51	Claystone	9.28E–4	53.4	–23.0	20.4	0.13	(400)	R
8R-1, 136-138	787.76	Claystone	3.37E–4	72.4	–58.2	22.0	0.04	(400)	R
9R-2, 5-7	797.54	Claystone	1.02E–3	57.0	–33.0	30.2	0.09	(300)	R
9R-4, 59-61	801.09	Claystone	4.86E–4	54.9	17.9	85.6	0.02	5	N
9R-4, 63-65	801.13	Claystone	5.30E–4	69.7	–20.7	35.2	0.04	10	R?
9R-4, 91-93	801.41	Claystone	5.50E–4	37.9	–10.8	105.6	0.01	50	R
10R-1, 82-84	806.42	Claystone	5.61E–4	1.3	–37.2	9.2	0.17	(300)	R
10R-2, 20-22	807.30	Claystone	3.47E–4	43.4	27.2	100.6	0.01	(550)	N
10R-3, 87-89	809.47	Claystone	2.11E–4	45.4	24.2	79.8	0.01	(400)	N
10R-4, 102-104	811.12	Claystone	2.88E–4	69.2	20.5			10	N
10R-4, 110-112	811.20	Claystone	1.42E–2	75.4	–5.8			10	R
10R-4, 124-126	811.34	Claystone	1.36E–4	67.5	–29.3	36.8	0.01	(500)	R
13R-3, 2-4	837.72	Claystone	8.79E–3	44.5	–47.4	20.6	1.19	(300)	R
13R-3, 81-83	838.51	Claystone	7.93E–3	60.4	—				
13R-3, 91-93	838.61	Claystone	3.06E–4	40.9					
14R-2, 81-83	846.71	Claystone	7.29E–2	47.6	14.5	137.1	1.48	(500)	N
14R-4, 82-84	849.72	Claystone	5.26E–2	6.5	–20.6	254.4	0.58	(400)	R
14R-5, 9-11	850.49	Claystone	1.88E–2	64.8	–40.6	94.1	5.57	(300)	R
15R-3, 82-84	857.82	Sandstone	6.92E–2	38.3	23.6	75.5	2.56	(400)	N
16R-1, 38-40	863.98	Chalk	3.87E–2	67.1	63.0	138.3	0.78	(500)	N
16R-2, 23-25	865.33	Sandstone	7.24E–2	–15.4	23.7	250.4	0.85	(400)	N
16R-2, 136-138	866.46	Sandstone	8.50E–3	12.3	1.38	13.82	1.72	(200)	N
16R-3, 16-18	866.76	Sandstone	6.81E–3	–14.8	–18.9	16.33	1.16	(200)	R
17R-1, 51-53	873.81	Grainstone	2.77E–4	86.5	–34.0			35	R
17R-1, 78-79	874.08	Grainstone	3.24E–4	–21.0	–27.3	32.5	0.03	(300)	R
17R-1, 89-91	874.19	Grainstone	1.40E–4	72.2	–13.1	19.1	0.02	(300)	R
17R-1, 113-115	874.43	Grainstone	3.33E–4	7.4	8.2	24.0	3.87	(300)	N?
21R-1, 20-22	911.80	Wacke	2.92E–4	19.4	4.4			20	N?
21R-1, 26-28	911.86	Wacke	2.45E–4	21.5	–14.5			30	R?
25R-1, 77-79	950.47	Wacke	2.92E–4	60.9	54.4	115.3	0.01	(200)	N
173-1070A-									
1R-1, 20-22	599.20	Claystone	3.62–2	55.7	30.9	45.4	2.23	15	N
1R-1, 27-29	599.27	Claystone	9.05E–3	75.6	1.7	33.6	0.75	15	N
2R-1, 65-67	609.35	Claystone	1.31E–2	59.3	25.6	55.0	0.66	10	N
2R-1, 133-135	610.03	Claystone	3.46E–2	63.4	66.8	67.8	1.42	5	N
3R-1, 102-104	619.32	Claystone	4.30E–2	44.4	14.3	71.6	1.68	5	N
4R-1, 113-115	629.03	Claystone	4.56E–2	68.5	–34.9	124.0	1.03	20	R
4R-2, 2-4	629.42	Claystone	5.50E–2	68.1	–24.9	126.6	1.21	20	R
5R-1, 16-18	637.76	Claystone	4.22E–2	38.2	–45.2	134.4	0.88	25	R
5R-1, 144-146	638.04	Claystone	5.80E–2	61.4	–3.5	185.2	0.87	10	R
5R-2, 7-9	639.17	Claystone	7.03E–2	57.0	2.3	214.0	0.92	10	R?
8R-1, 33-35	666.83	Breccia	2.07	66.3	60.3	1214.6	4.76	(400)	N
8R-1, 107-109	667.57	Peridotite	1.08	60.4	61.4	4079.0	1.00	(400)	N
8R-3, 33-35	669.74	Breccia	9.16E–1	–7.1	–7.3	3010.0	0.57	(400)	N
8R-4, 72-74	671.51	Breccia	1.09	–71.0	–15.7	5376.0	0.56	(375)	R
9R-1, 130-132	677.50	Gabbro	1.49E–1	67.2	–51.6	201.0	2.07	(300)	R
10R-1, 25-27	685.15	Peridotite	1.11	–35.4	–24.5	5292.0	0.58	(500)	R
10R-1, 72-74	686.62	Peridotite	2.09	59.1	51.4	39.7	0.80	(400)	N
10R-1, 91-93	686.81	Peridotite	1.52	32.3	21.9	4801.0	0.88	(400)	N
10R-1, 95-97	686.85	Peridotite	2.33	61.5	53.2	350.9	18.5	10	N
10R-2, 18-20	687.50	Peridotite	1.00	–64.4	–5.3	7321.0	0.38	(350)	R
11R-1, 71-73	696.21	Peridotite	1.49	64.9	40.9	273.3	15.2	(350)	N
11R-1, 81-83	696.31	Peridotite	1.70	–40.6	–41.2	7240.0	0.66	(400)	R

Table T1 (continued).

Core, section, interval (cm)	Depth (mbsf)	Lithology	NRM (A/m)	NRM-Inc (°)	ChRM-Inc (°)	χ (10^{-5} SI)	Q ratio	MDF/(T_b) (mT)/(°C)	Polarity
11R-2, 4-6	696.64	Peridotite	5.12E–1	21.9	—	9126.0	0.12		
11R-2, 29-31	696.89	Peridotite	7.68E–1	71.1	64.4	829.2	2.6	10	N
11R-2, 80-82	697.40	Peridotite	5.95E–1	–15.5	–5.0			(350)	R
11R-2, 99-101	697.59	Peridotite	5.38	–78.3	–30.4	551.0	27.3	(600)	R
12R-1, 21-23	705.31	Peridotite	8.76E–1	2.9	1.6	2325.4	1.05	(350)	N?
12R-1, 54-56	705.64	Peridotite	1.42	55.2	46.6	549.6	7.2	(525)	N
12R-1, 78-80	705.88	Peridotite	1.02	–1.1	–2.9	6330.0	0.45	(500)	R
12R-2, 5-7	706.01	Peridotite	1.16	–0.1	3.9	7731.0	0.42	(500)	R
12R-2, 40-42	706.36	Peridotite	5.85	63.2	–29.3	85.4	191.2	(550)	R?
12R-2, 83-85	706.79	Peridotite	1.22	79.2	–20.0	474.8	7.2	25	R?
12R-2, 109-110	707.05	Peridotite	8.29E–1	–4.7	–4.8	3754.0	0.62	(400)	R?
13R-1, 11-13	706.71	Peridotite	3.39E–1	27.7	47.0	1263.5	0.75	(350)	N
13R-1, 44-46	707.04	Peridotite	4.35E–1	–28.8	–11.4	1263.0	0.96	(200)	R
13R-1, 50-52	707.10	Peridotite	6.08	50.0	62.5	778.3	21.8	20	N
13R-1, 89-91	707.49	Peridotite	5.39E–1	–19.3	–10.8	4612.2	0.33	(450)	R
13R-2, 51-53	708.44	Peridotite	3.03E–1	–4.2	–3.1	1561.3	0.54	(300)	R
13R-2, 131-133	709.24	Peridotite	1.31E–1	0.9	–14.9	501.1	0.73	(300)	R
13R-3, 55-57	709.88	Peridotite	1.35E–1	–0.8	6.6	724.7	0.52	(200)	R?
13R-4, 13-15	710.70	Peridotite	6.44E–2	–10.7	–4.0	233.6	0.77	(350)	R?
13R-4, 68-70	711.25	Peridotite	9.39E–1	85.0	41.3	480.2	5.5	20	N
13R-4, 95-97	711.52	Peridotite	2.23	–0.7	–20.4	1295.5	4.81	15	R?
14R-1, 62-64	715.12	Peridotite	1.22	20.1	–15.1	5698.5	0.59	(500)	R
14R-1, 95-97	715.45	Peridotite	9.86E–1	–2.0	–1.0	1983.2	1.39	(200)	R?
14R-2, 21-23	715.89	Peridotite	2.50E–1	34.4	–10.2	5415.8	0.13	(500)	R
14R-3, 16-18	716.96	Peridotite	7.56E–1	16.8	8.1	6090.3	0.35	(500)	R?
14R-3, 62-64	717.72	Peridotite	1.07	–3.0	1.5	2890.1	1.03	(500)	R?
14R-3, 102-104	717.82	Peridotite	8.74E–1	–2.0	–1.5	4539.2	0.54	(400)	R?

Notes: NRM = natural remanent magnetization intensity, NRM-Inc = NRM inclination, ChRM-Inc = characteristic or stable remanent magnetization inclination after demagnetization, χ = low-field magnetic susceptibility, Q ratio = Koenigsberger ratio, MDF/(T_b) = median demagnetizing field/unblocking temperature, Polarity: N = normal, R = reversed. — = no data available.

Table T2. Hysteresis properties of minicore samples from the Leg 173 sites.

Core, section, interval (cm)	Depth (mbsf)	H_c (mT)	H_{cr} (mT)	H_{cr}/H_c	J_s (mAm^2/kg)	J_r (mAm^2/kg)	J_r/J_s
173-1068A-							
24R-1W, 92-94	924.12	12.4	25.3	2.04	181	27.7	0.153
26R-2W, 13-15	938.5	25.7	71.5	2.78	46.2	8.34	0.18
26R-4W, 18-20	941.11	11.2	50.4	4.5	296	20.6	0.07
173-1069A-							
7R-1, 45-47	777.25	22.9	35.9	1.57	14.3	5.59	0.391
7R-2, 95-97	779.25	23.5	34.3	1.46	12.9	5.10	0.395
7R-3, 60-62	780.4	22.2	43.8	1.97	4.0	1.56	0.388
173-1070A-							
8R-1, 107-109	667.57	13.5	25.1	1.86	496	95	0.192
10R-1, 25-27	685.15	12.8	24.2	1.89	1910	333	0.175
11R-1, 81-83	696.31	9.6	20.7	2.16	1940	227	0.117
13R-1, 44-46	707.04	7.61	19.8	2.60	6860	473	0.069
13R-4, 95-97	711.52	8.35	27.0	3.23	9.53	1.02	0.107
14R-2, 21-23	715.89	10.4	20.9	2.01	466	56.9	0.122

Note: J_s = saturation magnetization, J_r = saturation remanent magnetization, H_c = coercivity, and H_{cr} = remanent coercive force.

Table T3. Structural and magnetic data from the basement Subunit 1B from Hole 1068A.

Core, section, interval (cm)	VRM declination (°)	VRM inclination (°)	Working azimuths and dips of foliation (°)	Angle of rotation (°)	Reconstructed azimuths and dips of foliation (°)
173-1068A-					
25R-1, 78	351	65	NM	NM	NM
25R-1, 111	15	65	090/20	(–) 15	75/20
26R-1, 77	278	52	239/49	(+) 82	321/49
26R-1, 107	313	70	270/40	(+) 47	317/40
26R-2, 92	244	57	154/49	(+) 116	270/49
28R-1, 61	46	64	308/50	(–) 46	262/50
28R-1, 121	29	60	284/37	(–) 29	255/37
28R-2, 62	21	65	302/44	(–) 21	281/44
29R-3, 48	156	51	090/28	(–) 156	294/28
29R-3, 57	166	51	090/37	(–) 166	284/37

Note: (+) = clockwise, (–) = counterclockwise, NM = not measured.